Human-Robot Attachment System for Exoskeletons: Design and Performance Analysis

Journal Article

Author(s):
Zimmermann, Yves; Song, Jaeyong; Deguelle, Cédric; Läderach, Julia; Zhou, Lingfei; Hutter, Marco; Riener, Robert; Wolf, Peter

Publication date:
2023-08

Permanent link:
https://doi.org/10.3929/ethz-b-000608090

Originally published in:
IEEE Transactions on Robotics 39(4), https://doi.org/10.1109/TRO.2023.3268587

Human-Robot Attachment System for Exoskeletons: Design and Performance Analysis

Yves Zimmermann[1,3], Jaeyong Song[1], Cédric Deguelle[1], Julia Läderach[1], Lingfei Zhou[1], Marco Hutter[3,*], Robert Riener[1,2,*], and Peter Wolf[1,*]

***Abstract*—Exoskeleton robots found application in neurorehabilitation, tele-manipulation, and power augmentation. The human-robot attachment system of an exoskeleton should transmit all interaction forces while keeping the anatomical and robotic joint axes aligned. Existing attachment concepts were bounding the performance of modern exoskeletons due to insufficient stiffness for high-performance force control, time-consuming adaption processes, and/or bulkiness. Therefore, we developed an augmented attachment system for a recent fully actuated 9-DOF upper limb exoskeleton. The proposed system was compared to a conventional solution in a case study with four participants.**

The proposed attachment system lowered the relative motion between human and robot under static loads for all defined landmarks by $45\,\%$ on average. The occurrence of undesired contacts in the trials was mitigated by $74\,\%$, thus, improving conditions for closed-loop force control. Further, the proposed system adapted better to the user's anatomy facilitating more accurate alignment and less obstruction. On average, self-attachment took $43(8.3)$ s to don(doff). Thereby, the alignment of anatomic landmarks had typically less than $15\,\mathrm{mm}$ offset to a thorough expert alignment, making self-attachment eligible. The augmented attachment system and the insights gained by the case study are expected to enable improvement of the physical human-robot interaction of exoskeletons.

***Index Terms*—rehabilitation engineering, human-robot interaction, rehabilitation robotics**

I. Introduction

Per year, over 13.7 million people experience a stroke [1], [2]. Stroke survivors often suffer life-long deficits affecting their life on all levels. Next to stroke, many other neurological conditions can lead to a partial loss of motor control, *e.g.*, traumatic brain injury and Guillain-Barré-Syndrom [3]–[5]. Patients with these diseases can often regain some motor skills through the spontaneous and therapy-induced recovery of the neural system [6]. The best therapy outcome is expected with intensive therapy tailored to the needs of the patient [7]. To relieve therapists from repetitive and physically demanding labor of intensive therapy, robotic systems are deployed in neurorehabilitation. Thereby, high amounts of functional movement repetition and data-based intervention adaption can be provided [8]. To this end, the rehabilitation robot takes over the haptic interaction with the patient to assist, correct, or resist movements and assess the patient's performance by measuring movements and interaction forces. Robots with an exoskeleton structure are attractive tools for neurorehabilitation. Their structure can control all covered joints of the human individually to support more complex motor tasks typical for activities of daily living (ADL) with full posture control or assistance [8]–[11]. Further, hyperextension of the patient's joints is prevented by mechanical end-stops and the quasi collinear joint axes of the human and robot. However, exoskeletons also find application as assistive devices in daily live, and for occupational power augmentation in industrial or military applications. For precise interaction force and position control, fully controllable dynamics of the robot and the contact points to the human are required. In this case, the human's and the robot's joints should remain aligned during operation, as misalignment would cause undesired human joint loads [12]. Therefore, the human's torso and limb segments need to be consistently positioned, and best-constrained w.r.t. the corresponding robot links. Stiff constraints are preferred, to foster a high transmittable bandwidth in interaction force control, mitigate misalignment, and improve the accuracy of human joint angle estimation via robot joint angle measurements. For applications, where uncontrolled passive DOF are

Fig. 1. The augmented attachment system connects the ANYexo 2.0 with a user with two contact points at the upper arm and forearm each. The hand is attached such that the palmar side remains unobstructed to grasp objects.

This research was supported in part by the Swiss National Science Foundation (SNSF) through the National Centre of Competence in Research Robotics (NCCR Robotics).

[1] Y. Zimmermann, J. Song, C. Deguelle, J. Läderach, L. Zhou, P. Wolf, and R. Riener are with the Sensory-Motor Systems Lab, ETH Zurich, Zurich, Switzerland (e-mail: yvesz@ethz.ch)

[2] R. Riener is with the Spinal Cord Injury Center, Balgrist University Hospital, Zurich, Switzerland

[3] Y. Zimmermann and M. Hutter are with the Robotic Systems Lab, ETH Zurich, Zurich, Switzerland (e-mail: yvesz.ethz.ch)

* The three last authors contributed equally to this paper.

acceptable, exoskeleton solutions exist that do not require accurate joint alignment [13], [14]. At the same time, all interaction forces between the robot and the human should be transferred comfortably over these well-defined constraints of the human-robot attachment (HRA) system. Thus, the HRA concept is a key component of an exoskeleton nonetheless if the device is used for rehabilitation (*e.g.*, ANYexo [15], ArmeoPower and Locomat by Hocoma AG, Switzerland)), assistance (*e.g.*, MyoSuit by Myoswiss AG, Switzerland), or power augmentation (*e.g.*, Guardian XO by Sarcos, and EXO-O1 by Hilti AG).

Most related work on rehabilitation exoskeletons put little focus on the attachment system when developing a new robot design, while many mention the need for a more elaborate design of the HRA, *e.g.*, ANYexo [9], ARMin [11], CADEN [16], CAREX [17], Harmony [10] and MAHI [18].

A guideline for the kinematic design of upper limb HRA to achieve minimum parasitic interaction forces was presented by Jarrasse et al. [13] and a substantial body of studies regarding misalignment compensation mechanisms followed [19], [20]. However, while achieving a substantial reduction of parasitic interaction forces in static measurements, the increased deflections of the human joints w.r.t. the robot joints, caused by the added passive DOF, reduced the effect in dynamic application cases [13]. Investigations on HRA design addressing a more complete set of requirements can be found for lower limb devices [12]. We strove to identify the most restricting bottlenecks caused by attachment systems in the state of the art regarding the performance and usability of upper limb exoskeletons. Based on this analysis, an augmented attachment concept was developed that is presented and evaluated in this work.

A. Technical Requirements

Here, we focused on developing an attachment system for the 9-DOF, fully actuated upper limb exoskeleton ANYexo 2.0 [15], [21] (see section III-A). The main requirements and design goals for the ANYexo 2.0's attachment system were grouped into five categories (see Table I). However, these requirements are mostly not specific to this device. Therefore, requirements on the HRA for many other upper- and lower-limb exoskeletons with rehabilitation, occupational, military, or assistive purposes were comparable. Thus, the design choices for the HRA derived from this list of requirements will transfer well to other devices that share characteristics with the ANYexo 2.0.

Adaptability: The ANYexo was built to fit users from the 5th percentile female to 95th percentile male body height (see Table II). The attachment system should support this range regarding the positioning of the contact points and adaption to different arm circumferences. Hence, the attachment system should position arms of $70\,\mathrm{mm}$ to $111\,\mathrm{mm}$ diameter accurately and consistently w.r.t. the robot joints [22], [23].

Stiffness: The ANYexo employs 6-DOF interaction wrench measurement sensors at each contact point (Rokubi Mini, Bota Systems AG, Switzerland) to accurately measure interaction forces used for analysis and feedback control. These sensors can only accurately measure the interaction between the human and robot arms if any other contact point between the two arms is prevented. Therefore, the attachment system should constrain the arm w.r.t. the robot sufficiently stiff to avoid excessive misalignment and unintended contacts.

TABLE I
DESIGN GOALS AND QUANTITATIVE REQUIREMENTS (→) FOR THE ATTACHMENT SYSTEM.

Adaptability	
1.	size adaptable for 5th percentile female to 95th percentile male
2.	consistent joint alignment for all sizes
→	upper arm diameter of $70\,\mathrm{mm}$ to $111\,\mathrm{mm}$ [22], [23]
Stiffness	
3.	low relative deflection between human and robot under load
4.	no unintended contact points between human and robot
Repeatability	
5.	consistent joint alignment independent of therapist
6.	self-attachment possible with comparable joint alignment
7.	re-attachment efficiently repeatable after initial alignment
→	independent donning in $\leq 120\,\mathrm{s}$; doffing in $\leq 30\,\mathrm{s}$
→	less than $0.02\,\mathrm{m}$ deviation from initial alignment
Usability	
8.	open concept for accessibility by severely affected users
9.	suited for one handed fastening during self-attachment
10.	enable grasping of objects and interactions with the body
11.	encourage training torso stability
12.	easy to use and understand
→	no tools
→	no additional items
Low averse effects on robotic system	
13.	little occupied volume
14.	lightweight
15.	sufficient comfort

A stiffer connection between the human and robot arms mitigates misalignment under load. Thereby, the parasitic interaction forces acting on the joints of the user are reduced as well, assuming a good initial alignment. These undesired forces could cause joint pain and limit the range of motion (ROM) [12]. Misalignment mitigation under load is less significant for systems that employ passive DOF for misalignment compensation [13] compared to systems that prevent passive DOF like the ANYexo 2.0.

Additionally, a stiff human-robot connection promotes a large bandwidth for interaction force control with the device. Our experience with a conventional attachment system on the first prototype of ANYexo indicated that the torsional stiffness of the upper arm constraint should be significantly increased to avoid excessive deflections of the glenohumeral and elbow joints.

Repeatability: Adapting the size of the ANYexo thoroughly to a new user takes around $15\,\mathrm{min}$ to $20\,\mathrm{min}$ [9]. After this initial setup procedure, the length settings can be measured and documented. To use the therapy time efficiently, we determined the re-attachment of a user on the robot configured with the documented settings should not take longer than $2\,\mathrm{min}$ and achieve a comparable alignment as during the initial setup. This re-attachment should be possible for all instructed therapists, not only those who performed the initial setup. To increase the autonomy of patients in robot-assisted therapy, patients with one able arm should be able to self-attach and -detach from the robot with accuracy and speed comparable to

the therapist alignment. We determined, the detachment from the robot should not take longer than $30\,\mathrm{s}$ to release the patient quickly if required.

Usability: Severely affected patients constitute a significant part of ANYexo's target population. These patients often struggle to maneuver their hands and arms through confined spaces, *e.g.*, due to tonic spasticity. Hence, the attachment system should be accessible without the necessity to stick the limb through a confined space, *e.g.*, closed ring. To allow self-attachment, the attachment system should only require one hand to fasten the attachment mechanisms.

To promote the transfer of learned skills during therapy to daily life at home, therapy involving manipulating real objects should be possible with the device. Hence, the attachment mechanism at the hand should allow grasping objects. The attachment system should be easy to use with brief instructions to promote its adoption in clinics. Therefore, neither tools nor additional items (*e.g.*, custom cushioning) should be required to adapt the attachment system to the size of a user and fasten it. The torso attachment system should prevent compensatory movements with the torso and slumping down during longer sessions. Further, all consulted therapists agreed that training torso stability during arm function training is essential. Therefore, the torso should be constrained such that training of torso stability is not inhibited during the training of arm movements.

Low averse effects on robotic system: The attachment system should restrict the system's performance as little as possible. Hence, the attachments should have a minimum footprint (*i.e.*, volume around the arm) to avoid a reduction in ROM. Furthermore, the more lightweight the robot is, the less inertia will be felt when the robot renders free-space, as only up to $50\,\%$ of the inertia can be compensated by the feedback control laws [24]. Further, the mass of the attachment mechanism is on the human side of the interaction force sensors. The higher the mass, the higher the distortion of the interaction force measurement caused by the inertia of the attachment mechanism. Therefore, the attachment mechanisms on the arm should be lightweight. Typical therapy sessions last for $20\,\mathrm{min}$ to $60\,\mathrm{min}$. During a large fraction of this time, the patient will be attached to the robot and experience various interaction forces. The attachment system should be designed such that transmission of these forces does not cause remarkable discomfort and skin irritations.

B. Project Goal

Thus, we strove to develop an augmented attachment system for the therapy exoskeleton ANYexo, that addresses all requirements and design goals summarized in Table I. Such a system would mitigate misalignment during donning and operation, facilitate high performance closed-loop interaction force control using measured interaction forces, be convenient and efficient to use, and offer more autonomy for patients in using the device. In a case study on four participants we investigate the performance of the augmented attachment concept (AAC) compared to a conventional attachment system regarding the technical requirements. Particularly, we present a thorough investigation of the relative movement between human and robot during typical load cases.

II. State of the Art

A. Conventional Attachment Systems

Many academic devices (*e.g.*, ALEX [25], ANYexo [9], ARMin [11], CADEN [16], Harmony [10], and HUMA [26]) and commercially available devices (*e.g.*, ArmeoPower and Locomat by Hocoma AG, Switzerland and MyoSuit by MyoSwiss AG, Switzerland) have applied a HRA system that was based on a similar concept: A chair with or without a backrest to position the torso. For the arm attachment, a u-shaped, rigid base on both the upper arm and the forearm was used combined with textile straps to fasten the arm segments to the u-shaped base (see Fig. 3). In addition, a grip was provided for the hand constraint.

The u-shaped base of the HRA allowed the user to get into the device without maneuvering the hand through a confined space in contrast to o-shaped base designs as deployed by (*e.g.*, CAREX). The larger the circle segment the U-shaped base encloses, the more lateral load can be transferred (*e.g.*, ARMin). However, individualized cushioning or u-shaped base structures are needed to adapt these cuffs to different user sizes. Mostly, the same base design was used for all users leading to the HRA occupying a large volume around thinner arms. In case the base structure is almost flat, the textile straps suffice to adapt to different user sizes at the cost of lower stiffness as deployed on (*e.g.*, ArmeoPower). Most robots were equipped with one HRA placed at the middle or distal end of the upper arm and the forearm. Thereby, the force transfer was concentrated to one location, which may have limited the transmission of torque as elaborated by [13]. On Harmony, Kim *et al.* deployed a concept with two HRA on the upper arm to increase the rotational stiffness of the connection by the increased lever arms of the contact pressure.

B. Specialized Attachment Systems

Specialized, more complex HRA design concepts have addressed the adaptability to different body sizes while still providing a relatively large stiffness of the human-robot connection.

Inflatable HRA adapt the shape and distribute the load evenly over the contact surface [27]–[30]. However, the constant pressure on the human's soft tissue can inhibit blood circulation and restrict muscular contraction [31].

Several related works investigated HRA concepts which can be manually adapted to the user's arm shape (*e.g.*, Restrepo-Zapata *et al.* [32], Chen *et al.* [33], or Chui *et al.* [34]) or incorporate custom, thermoformed shells (*e.g.*, Vitiello *et al.* [35]). The drawback that they have in common is a time-consuming adaption procedure, either for manual adaption of the setting screws or to manufacture and handle the custom parts. Some of these designs require maneuvering the arm through a confined space, and occupy a large footprint as their outer shape does not adapt to the user's arm.

Exoskeletons for occupational and defense applications mostly connect to the human via the end-effector of the robot only, as guidance and monitoring of the joint positions was typically not required, *e.g.*, Guardian XO by Sarcos, EXO-O1

by Hilti AG, and BLEEX [36]. However, for future developments that strive towards fast and powerful exoskeletons improved guidance of the limbs could be desirable to mitigate the risk of undesirable loads on the human joints.

Torso harnesses were proposed to constrain the upper torso movements, *e.g.*, by Kim *et al.* [10]. However, a torso harness can restrain breathing if fixed over the chest or limit the ROM if back-pack-like straps are used. Further, the harness will prevent patients from training torso stability.

C. Limitations of Related Work

Human-robot attachment systems received relatively little attention compared to kinematics and actuation of exoskeletons, despite being similarly relevant for the overall system performance. Most devices, particularly the industrial ones, resort to u-shaped shells with textile straps due to their simplicity, reliability, and easy use. However, there are highly specialised attachment systems that trade complexity in construction and use for improved alignment and comfort. Nevertheless, a system that satisfactorily fulfills all our requirements and design goals has not been presented yet.

Adaptability: All presented systems allow to adapt the size to different users. However, for the systems that provide sufficient stiffness in the constraint, this adaption involves an exchange of customized parts (*e.g.*, shells or cushioning) or time-consuming tuning.

Stiffness: HRA with significant elastic deformation accommodate different arm sizes and shapes, *e.g.*, customized foam or elastic bushings, achieve a too low stiffness for high performance interaction force control as undesired contact points may not be prevented and the transmissible bandwidth is restricted. Using individualized layers of foam will even lead to an inconsistent stiffness for different arm diameters.

Repeatability: Using customized parts and settings increase the risk of mistakes during the setup. The authors are unaware of any specific design measures to ensure alignment accuracy when re-donning the devices presented by related work.

Usability: Concepts involving closed structures like the one presented by Restrepo-Zapata *et al.* [32] are not suitable for patients with strong spastic tone. Some mechanisms such as the one used on ASSISTON and CAREX-7 [33], [34] are likely to take a long time to don and doff, particularly when self-attaching. Most attachment systems of rehabilitation exoskeletons were not particularly developed to allow for grasping of real objects. Still, with some devices, real object manipulation could be demonstrated, *e.g.*, Harmony [10]. Assistance to prevent compensatory movements without inhibiting training of torso stability has not been presented so far.

Low Constraints on System: Many attachment systems in the state of the art have been built with fixed outer structures, *e.g.*, [11], [32]–[35]. Thereby, users with thinner arms will experience an unnecessary reduction of the ROM.

III. Methods

A. Exoskeleton Robot

The ANYexo, a fully actuated exoskeleton, has been built as tool for neurorehabilitation (see Fig. 1). The first prototype without wrist degrees of freedom was presented by Zimmermann *et al.* in [9]. This device was later equipped with stronger actuators and a wrist module [15]. The robot covered all relevant degrees of freedom (DOF) of the human shoulder and arm with a 2-DOF sternoclavicular joint (SC), 3-DOF glenohumeral joint (GH), 1-DOF elbow joint (EB), and 3-DOF wrist (WR) (see Fig. 2a). The kinematic structure of the robot covered almost the full active ROM of humans. The exoskeleton was adaptable for users of the 5th percentile female to 95th percentile male population. The shoulder and elbow joints exhibited series-elastic actuators, while the wrist used pseudo-direct drives with $77\,\mathrm{N\,m}$, $39\,\mathrm{N\,m}$, and $23\,\mathrm{N\,m}$ peak torque, respectively. Thereby, the robot was strong enough to provide mobilization and strength training. The speed and kinematic structure of the robot allowed training with velocities up to double the speed required in activities of daily living as reported by Rosen *et al.* [37].

The series-elastic joints could measure the joint torque over the deflection of the spring. In contrast, the pseudo-direct joints could estimate the joint torque over the current due to the drive's low friction and transmission ratio. Each joint was equipped with encoders to measure the angle. 6-DOF force/torque sensors (Rokubi, Bota Systems AG, Switzerland) were mounted at the upper arm, the forearm, and the hand attachment points to measure the interaction forces between the human and robot arms. The measurement and control update frequency of the robot was $800\,\mathrm{Hz}$.

For the experiments of this work, three types of controllers were used: *position control*, *free space*, and *damped free space*.

In *position control* mode, a static reference position or reference position on a trajectory was tracked by the PID position controller implemented on the motor controllers. This mode was used to move the robot to different postures.

In *free space control*, the robot compensated for its gravity, Coriolis, and centrifugal terms, by commanding the reference joint torques to the motor controllers as described in [9]. Only the SC joints were controlled by an impedance controller to follow a desired shoulder rhythm w.r.t. the plane orientation of the upper arm in world frame.

In *damped free space control* the robot rendered a damping of $1.1\,\mathrm{N\,m\,s\,rad^{-1}}$ on the SC, GH, and EB joints and $0.2\,\mathrm{N\,m\,s\,rad^{-1}}$ on the WR joints in addition to the *free space controller*.

B. Kinematic Model and Alignment

The primary function of the HRA was to connect the human limb segments with the corresponding robot's segment. The first of these segments were the torso and the base of the robot that define the location of the $\mathrm{SC_{H/R}}$ joints of the two systems, human (H) and robot (R). The second segment were the shoulder girdle between the $\mathrm{SC_{H/R}}$ and $\mathrm{GH_{H/R}}$ joints.

The third segment was the upper arm between the $\mathrm{GH_{H/R}}$ and $\mathrm{EB_{H/R}}$ joints. The fourth was the forearm between the $\mathrm{EB_{H/R}}$ and $\mathrm{WR_{H/R}}$ joints. However, the forearm was split in a proximal end where the ulna and the radius move with the elbow joint and a distal part where ulna and radius rotate with the wrist in pronation and supination. The fifth segment was the hand as the end-effector of both systems.

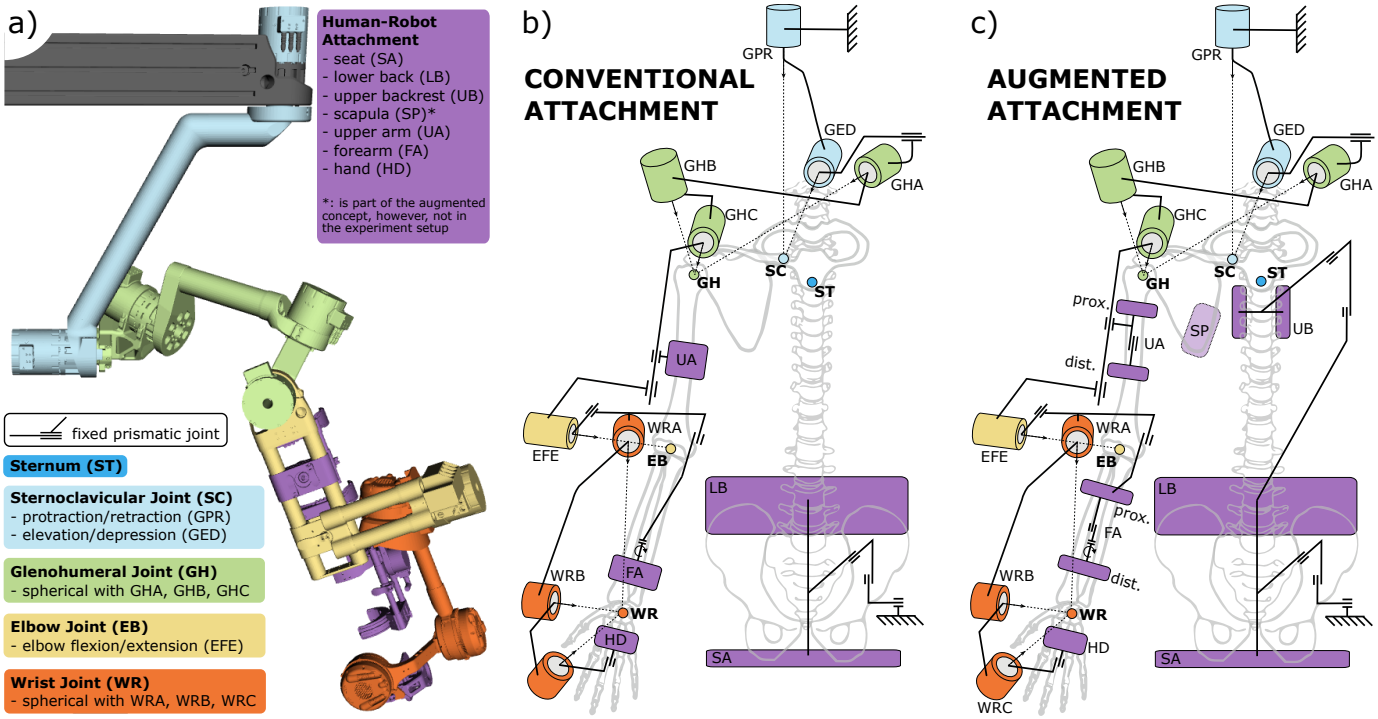

Fig. 2. Kinematic structure of the robot and the attachment concepts. a) Rendering of the moving mass of the robot with links colored to identify the joint group; b) conventional attachment system; c) augmented attachment system.

The position of the robot joints (*e.g.*, robot glenohumeral joint position $\boldsymbol{p}_{\mathrm{GH}}^{R}$) should be aligned as accurately as possible with the position of the human joints (*e.g.*, human glenohumeral joint position $\boldsymbol{p}_{\mathrm{GH}}^{H}$). Any misalignment of the robot between the corresponding joints of the two systems after the alignment procedure (*e.g.*, $\Delta\boldsymbol{p}_{\mathrm{GH}} = \boldsymbol{p}_{\mathrm{GH}}^{R} - \boldsymbol{p}_{\mathrm{GH}}^{H}$) will lead to parasitic interaction forces that do not act in the direction of the DOF of the system [12]. Such parasitic forces can be mitigated by careful alignment. However, a certain misalignment will always remain in clinical practice as a trade-off to the time effort has to be made, and the human joints are not perfect hinge or spherical joints. Adding passive DOF as used on the exoskeleton LIMPACT would compensate for the misalignment [14], [20]. However, passive DOF on the robot would create uncontrollable dynamics that should be prevented for high-quality interaction force control [24]. Compliance in the attachment system will also mitigate these parasitic forces at the cost of slipping or tensioned contact points. Adding more compliance is not solving the challenge, as a more compliant HRA will cause more extensive misalignment under load. Hence, the optimum stiffness is a trade-off between compliance to misalignment and high stiffness that benefits alignment under load, avoiding undesired contact points, and a high force transfer bandwidth between human and robot arm (*i.e.*, interaction force control).

To align the exoskeleton to the human, the position of the torso (*i.e.*, the SC joint) and the lengths of the arm segments of the exoskeleton had to be adapted to the humans anatomy. For the SC alignment, the torso of the user was positioned by changing the seat and lower backrest position (see Fig. 2). Therefore, the ANYexo had prismatic joints that were fixed during operation of the robot and could be manually adapted for alignment.

However, setting the length of the arm segments is not enough to ensure alignment. Arms with different circumferences have to be positioned at the correct distance to the exoskeleton structure (x-direction, direction definitions see Fig. 5), such that the joints of human and robot match. For example, attaching a 5th percentile female and a 95th percentile male upper arm (see Table II) to a u-shaped shell cuff system would lead to an offset of the GH and EB joints of the two arms of more than $20\,\mathrm{mm}$ if no foam is used to increase the distance between the thin arm and the base of the u-shaped structure. This offset would add to the other causes of static misalignment and to deflections resulting from loading the contacts. To solve this issue, we developed a mechanism that positions arms of different widths at a consistent position with minimum effort (see Section III-E).

C. Conventional Attachment Concept (CAC)

The conventional attachment system comprised the torso and upper arm HRA from the earlier version of the ANYexo [9]. We considered this attachment system as a conventional solution as it was directly adopted from the HRA solution on ARMin III [11], which was frequently used for clinical studies (*e.g.*, [8]), and on ArmeoPower (Hocoma AG, Switzerland), which was the leading commercial device of this type. For ANYexo [9] the upper arm cuff was designed slightly wider than on the ARMin and ArmeoPower improve the transmission of torques produced by the sternoclavicular joints. The forearm and hand constraints were updated to fit the requirements of the added wrist degrees of freedom (see Fig. 2 and Fig. 3).

Torso: The torso attachment consisted of a chair (VELA, Denmark) with a seat and a lower backrest just above the seat at the height of the lumbar vertebrae. This concept has been

frequently reported in the state of the art, *e.g.*, by Keller et al. and Mihelij et al. [38], [39], and mainly constrains the pelvis. The seat was adjustable in height. For the adjustment in anterior/posterior and lateral direction, the chair had wheels that could be locked. Aluminum rails with scales were used to measure and set the position of the chair, so that settings were repeatable.

Arm: The upper arm (UA) was attached by one contact mechanism around the middle of the humerus (see Fig. 2). The contact mechanism consisted of a u-shaped base (printed polyamide 12) with $0.1\,\mathrm{m}$ width in z-direction of the attachment and $0.09\,\mathrm{m}$ inner diameter (see Fig. 3). Hence, a cylinder with an average upper arm circumference (see Table. II) could just be fitted to the conventional cuff without additional cushioning. The HRA was adapted to smaller arm diameters by additional foam cushioning. Two textile belts fastened the arm with Velcro. A prismatic joint could adapt the position of the UA-HRA between the GH and EB joint.

The forearm (FA) was attached by an attachment mechanism close to the wrist on the forearm. To allow for the pronation and supination movement, this mechanism comprised a circular rail that was pulled towards the rail rollers by a Dyneema cable and the tensioning mechanism (see Fig. 4 bottom middle). The Dyneema cable was mounted to the ends of the circular rail and was guided on the circumference of the rail. Thereby, a stiff, lightweight, and low profile remote center of rotation mechanism was realized, allowing a rotation of $115°$. A lock pin allowed to block the rotation of the cuff for easy donning and fastening of the HRA in neutral pro-/supination rotation. To fasten the HRA, a textile belt with Velcro was used. Individualized cushioning to adapt the attachment to thinner arms was seldomly required due to the low difference in ulna and radius thickness between users and the low soft tissue content. A prismatic joint could adapt the distance of the forearm HRA to the WR joint.

Hand: The typical hand attachment for exoskeletons would consist of a handle that the user grasps. Such a hand HRA was available for ANYexo. However, an alternative hand attachment was designed to allow the user grasping objects and interacting with the own body. This attachment mechanism was used for both the AAC and the CAC system during the experiments of this study. This alternative hand HRA consisted of a slightly bent aluminum plate with $5\,\mathrm{mm}$ cushioning that contacts the hand on the dorsal side at the height of the metacarpals. Furthermore, a $25\,\mathrm{mm}$ wide textile strap with Velcro over the palmar side of the hand pulled the hand towards the plate on the dorsal side. The angle of the strap w.r.t the longitudinal direction of the hand could be adapted. An angle of $90°$ constituted a good trade-off between low slip of the attachment system and comfort. To increase the comfort, the belt would be rotated distally at the thumb side. The hand HRA location w.r.t. the WR joint could be adapted to the size of users by a prismatic joint that adapted hand length and thickness simultaneously.

D. Augmented Attachment Concept (AAC)

1) Torso: The AAC used the same components as the CAC to constrain the pelvis. Undesired lateral and anterior/posterior shifts were often observed during the use of ANYexo, and ARMin and reported by therapists working with ArmeoPower. However, the therapists wished an upper torso constraint which allows training of torso stability and reduces feeling of constriction. Therefore, we introduced a haptic reference structure for the upper torso consisting of two vertical contact bars at the height of the first to the fifth thoracic vertebrae. The two bars were placed $40\,\mathrm{mm}$ horizontally apart to avoid any pressure on the spinous process and the medially rotated scapula in the nominal position. Users got instructed to stay in contact with the backrest by leaning lightly against it. Thereby, an anterior shift will be noticed immediately. Further, a lateral shift would be detected by an asymmetric feeling of pressure w.r.t. the spine, particularly when pressure on the spinous process is applied.

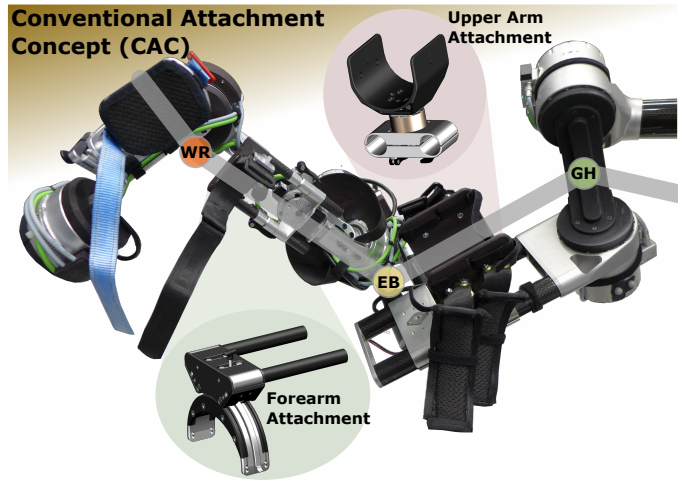

Fig. 3. Conventional human-robot attachment system of forearm and upper arm with opened textile belts. The custom cushioning of the upper arm attachment is not displayed. The same hand attachment mechanism as for the AAC was used (see Fig. 4). The location of the arm is indicated with a gray stick figure and color coded joints.

2) Arm: When using the ANYexo with the SC joints rendering free space, *i.e.*, letting the user define the GH translation, the CAC with only one contact point at the upper arm would lead to large deviations of the human and robot GH joints and even result in harmonic oscillations between the SC and GH joint angles (see video[1]). These harmonic oscillations were a consequence of low torsional stiffness connecting the human and robot upper arm. Later experiments have shown, that increasing the stiffness of the HRA changes the coupled human-robot dynamics sufficiently to prevent activation of the harmonics during operation of the robot (*i.e.*, shift of the dynamics to a not excited frequency band) [15]. Furthermore, contact between the lateral epicondyle (elbow) and the exoskeleton structure was frequently established. The bottleneck of the HRA's stiffness was the low torsional stiffness perpendicular to the longitudinal axis of the humerus, *i.e.*, x- and y-direction.

To achieve a higher torsional stiffness, either the translational stiffness of the connection could be improved or the width of the contact (*i.e.*, lever arm). The translational stiffness in x- and y-direction of an attachment location $k_{\mathrm{x/y}}$ is the serial

[1]https://youtu.be/RgazsS3NYpU

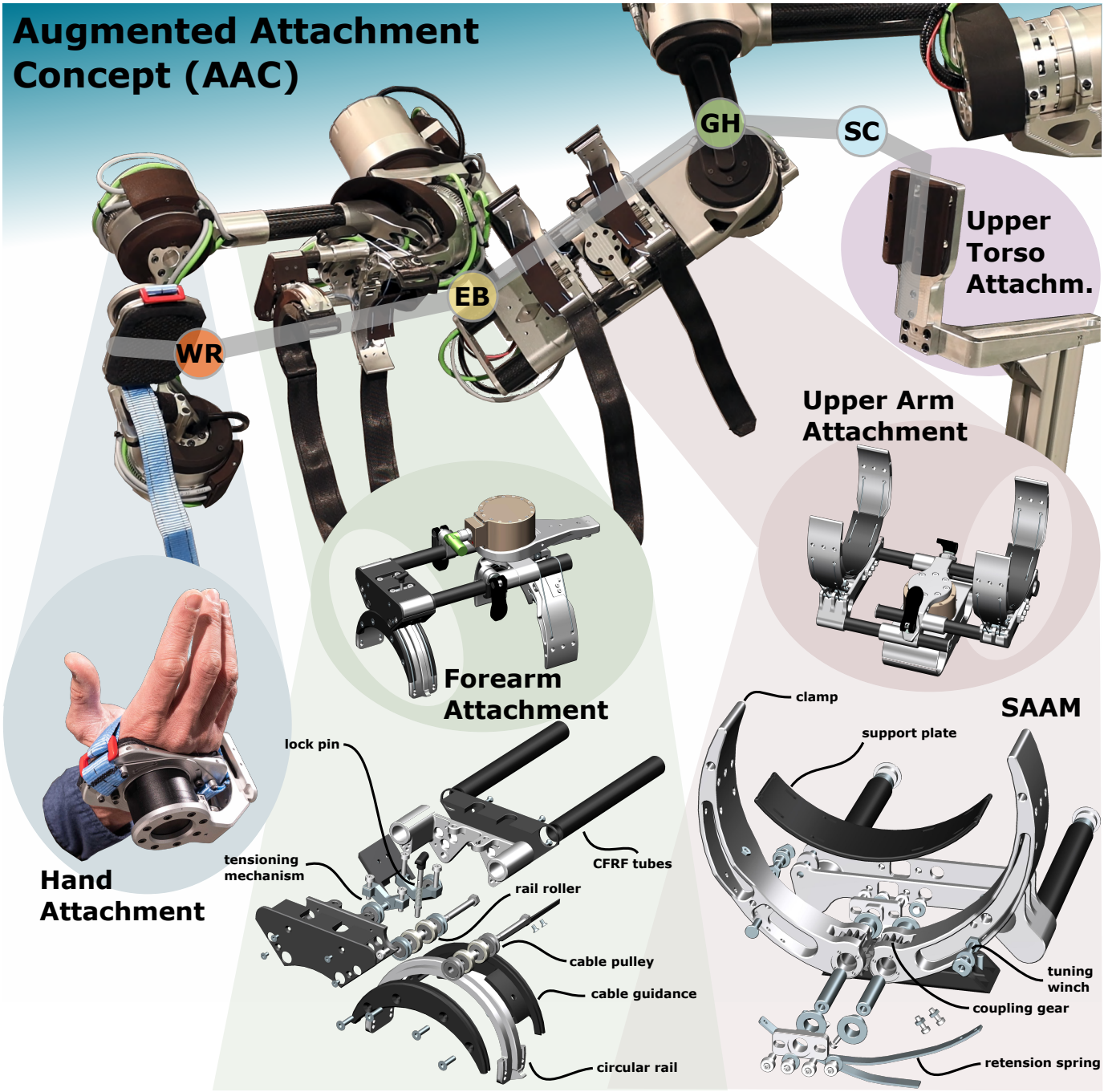

Fig. 4. Augmented human-robot attachment system on ANYexo 2.0 (top) with open textile belts. The location of the arm is indicated with a gray stick figure and color coded joints. Renderings of the isolated attachment mechanisms with explosion renderings of the SAAM (right bottom) and the distal forearm attachment mechanism (center bottom).

stiffness of the fat tissue k^{fat} and muscle tissue k^{muscle} between the attachment mechanism and the human bone as well as the attachment mechanism's stiffness k^{mech}

$$\frac{1}{k_{\text{x/y}}} = \frac{1}{k^{\text{fat}}_{\text{x/y}}} + \frac{1}{k^{\text{muscle}}_{\text{x/y}}} + \frac{1}{k^{\text{mech}}_{\text{x/y}}}. \tag{1}$$

The Young's moduli of fat and muscle are approximately $E_{\text{fat}} = 21\,\text{kPa}$ and $E_{\text{muscle}} = 87\,\text{kPa}$, respectively [40]. The average thickness of fat tissue can be assumed quite consistent with $l_{\text{fat}} = 3\,\text{mm}$ [41]. The thickness of the muscle tissue l_{muscle} varies significantly between users. However, it can be estimated considering the bone diameter [42] and arm diameter [22]. Due to the high water content, the soft tissue can be approximated as incompressible, therefore the Poisson's ratio was $\nu = 0.5$.

Using these values the linear stiffness of the soft tissue was computed by

$$k^{\text{n,c}}_{\text{x/y}} = \frac{E^{\text{n}} A^{\text{c}}}{l^{\text{n}}} \qquad k^{\text{n,c}}_{\text{z}} = \frac{E^{\text{n}} A^{\text{c}}}{2 l^{\text{n}} (1+\nu)}, \tag{2}$$

where A^{c} was the contact area under pressure corresponding to contact point c. The variables l^{n} and E^{n} were the thickness and the Young's modulus of the tissue layer n, respectively. The resulting estimated soft tissue stiffness at the upper

arm for an average adult with a $100\,\mathrm{mm}$ wide attachment mechanism was approximately $k_{\text{SoftTissue,100}} = 10\,\mathrm{N\,mm^{-1}}$, which was generalized to the soft tissue stiffness per width $\hat{k}_{\text{SoftTissue}} = 100\,\mathrm{kN\,m^{-2}}$. For this estimation we assumed that the average of the bone diameter (*i.e.*, $19.3\,\mathrm{mm}$ [43]) and the full arm diameter (see Table II) contributed to the load transfer.

To achieve high stiffness in the overall connection, k_{mech} of the contact was designed such that it has negligible influence on (1). Thereby, the translational stiffness $k_{\text{trans}} \approx \hat{k}_{\text{SoftTissue}} w_{\text{section}}$ of the HRA mainly depended on the width of the total contact area w_{section}.

The torsion stiffness k_τ in x- and y-direction of the HRA could be estimated by splitting the attachment along the z-axis into two sections

$$k_\tau = 0.25 d_{\text{section}}^2 \hat{k}_{\text{SoftTissue}} w_{\text{section}} \tag{3}$$

where d_{section} was the distance between the center of the two segments and w_{section} was the width of both segments together. Hence, by increasing d_{section} a higher torsional stiffness could be achieved even when reducing the width of the contact areas. Further, the contact forces to establish a certain torque were lower if d_{section} was larger.

Therefore, we split the upper arm HRA into one close to the proximal and one close to the distal part of the upper arm with each a width of $0.03\,\mathrm{m}$. With this split and the narrower contacts, the contact locations could be placed at the proximal and distal end of the biceps brachii, allowing it to expand during flexion.

For the forearm, a second contact point at the proximal side was used in addition to the distal contact location of the CAC. Thereby, the same benefits as discussed for the upper arm are achieved. Additionally, the improved constraint of the forearm close to the elbow contributed to the overall stiffness of the upper arm attachment due to the force coupling over the elbow joint.

For the two contact mechanisms of the upper arm and the proximal contact mechanism of the forearm, the Self-Adapting Attachment Mechanism (SAAM) was used (see section III-E) to assure consistent positioning of the joints for all arm circumferences. For the upper arm and the forearm, the geometry of the mechanism was optimized for the least variation in distance h_A, when attaching arm circumferences of the 5th percentile female to the 95th percentile male (see Table II).

3) Hand: The same hand attachment was used for the AAC as for the CAC.

E. Self-Adapting Attachment Mechanism (SAAM)

The main requirements for the SAAM (see Fig. 5) were:

- the mechanism should place the center of cylinders with radii in a selected range $\left[R_{\text{A}}^{\text{small}}, R_{\text{A}}^{\text{big}}\right]$ at the same distance h_A to the base structure
- no manual adaption except for the fastening procedure should be required
- no customized or exchangeable parts
- the mechanism should not require maneuvering the limb through a confined space

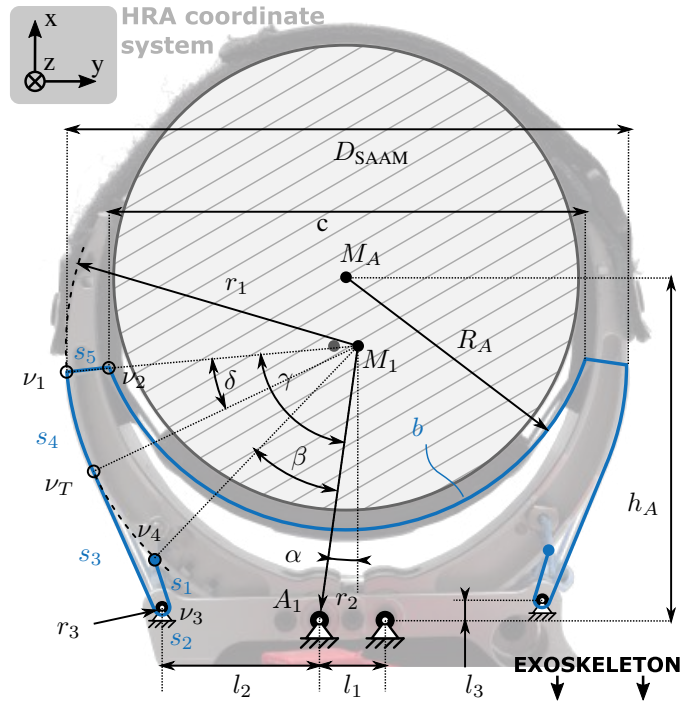

Fig. 5. Kinematic structure of the self-adapting attachment mechanism (SAAM) and coordinate system definition for HRA. The string segments (blue) are symmetric on the right-hand side. Segment s_2 is the arc length of the string in contact with the circular rerouting point. The x-direction points away from the exoskeleton structure and is the direction from which the cuff is approached when donning. The z-direction is parallel to the connecting line between adjacent joints and points in the direction of the distal joint. M_A is the middle of a cylinder (gray hatched) attached to the SAAM. A_1 is the rotation point of the clamp 1. The distance h_A between M_A and A_1 should remain constant when attaching cylinders of different radius R_A. D_{SAAM} is the diameter of the SAAM system measured at the outermost point of the clamps.

- the outer diameter (footprint) of the mechanism should adapt to the diameter of the human arm
- fastening and opening the mechanism should be possible using only one hand
- the closed the SAAM should constrain the attached arm in x- and y-direction with a closed kinematic structure to facilitate lightweight design.

The SAAM consisted of two aluminum clamps that were mounted to the base structure such that they could pivot around points A_1 and the mirrored equivalent (see Fig. 5 and Fig. 4 bottom right). A pair of retention springs was used to keep the clamps apart to allow easy access to the attachment system. The movement of the two clamps was constrained by coupling gears such that they rotated with inverse angles. The fastening system consisted of a textile belt with Velcro mounted to one of the clamps and a rerouting loop mounted to the other clamp. If the system was fastened the two clamps were pulled towards each other until both were in contact with the arm. Thereby, the arm was constrained in y-direction. Simultaneously, the footprint of the cuffs adapted to the diameter of the arm.

To support the arm in negative x-direction, a lower support structure (printed polyamide-12) was suspended by two strings. These strings were routed through holes in the clamps (see Fig. 5 ν_1 and ν_2). Up to the point ν_T, the strings were in contact with the surface of the clamps with a circular shape of radius r_1. The strings were rerouted by a steel pin at ν_3 and

attached to the clamp at ν_4 (see Fig. 5). A tuning winch on each clamp allowed to tune the string length after assembly. The geometry of the clamps and the location of the rerouting points were designed such that fastening the cuffs would shorten the length of the string between the clamps. Thereby, the support plate was pulled upwards keeping the center of the attached arm at a consistent position w.r.t. the base. For a given range of cylinder radii R_A and a value for the desired distance h_A, a suitable geometry (*i.e.*, $l_1, l_2, l_3, l_4, s_5, s_{\text{tot}}, r_1, r_2, r_3, \beta$, and γ) can be derived by constraint optimization using the kinematic description of the mechanism

$$\begin{aligned} h_A &= r_2 \cos(\alpha) - \cos(\alpha+\gamma)(r_1 - s_5) + \sqrt[2]{R_A^2 - 0.25c^2} \\ c &= 2\sin(\alpha+\gamma)(r_1 - s_5) + l_1 - 2r_2 \sin(\alpha) \\ b &= s_{\text{tot}} - 2(s_1 + s_2 + s_3 + s_4 + s_5), \end{aligned}$$

where b can be numerically solved for α using the the description of the string segment lengths s

$$\begin{aligned} s_1 &= \sqrt[2]{\left(r_3 - l_2 + r_1 * \sin(\alpha+\beta) + r_2 \sin(\alpha)\right)^2 + \hat{s_1}^2} \\ \hat{s_1} &= r_1 * \cos(\alpha+\beta) - l_3 - r_2 \cos(\alpha) \\ s_2 &= \pi r_3 \\ s_3 &= \sqrt[2]{\left(r_1 \cos(\alpha - \delta + \gamma) - l_3 - r_2 \cos(\alpha)\right)^2 + \hat{s_3}^2} \\ \hat{s_3} &= l_2 + r_3 - r_1 \sin(\alpha - \delta + \gamma) + r_2 \sin(\alpha) \\ s_4 &= \delta R_A, \end{aligned}$$

where δ is a function of α

$$\begin{aligned} \xi &= \sqrt{(l_2 + r_3 + r_2 \sin(\alpha))^2 + (l_3 + r_2 \cos(\alpha))^2} \\ \delta &= \gamma - \arccos\left(\frac{r_1}{\xi}\right). \end{aligned}$$

All SAAM of the prototype used for these experiments were equipped with $2.5\,\text{mm}$ neoprene cushioning at the contact locations. In contrast, typical conventional attachment systems involve individualized cushioning (*e.g.*, ARMin [11]) or mostly textile attachments (*e.g.*, ArmeoPower, Hocoma AG, Switzerland) that are likely to exhibit inconsistent and low stiffness constraints. Dyneema strings (DSM, Netherlands) with 2mm diameter were used for the strings of the SAAM.

IV. Experiment on Attachment Mechanism Properties

Three cylindrical dummy arm segments with different diameters ($70\,\text{mm}$, $90\,\text{mm}$ and $111\,\text{mm}$) representing the 5th percentile female, average, and 95th percentile male human upper arms (see Fig. 8) were used to determine the stiffness and kinematic properties of the attachment mechanism itself. For this experiment the attachment system was rigidly fixed to a stiff test bench.

The following procedure was repeated for each dummy arm segment with the AAC's SAAM and for the small dummy arm segment with the CAC's u-shaped attachment for the upper arm. The dummy was attached to the HRA. A string was routed through its middle to apply forces with a spring scale. A force of $100\,\text{N}$ was applied in positive x- and y-direction, while the deflection of the dummy arm segment's center was measured with the motion capture system. Thereby the mechanical stiffness $k_{\text{mech,i}}$ could be calculated.

TABLE II
Study participant characteristics and representative human characteristics according to [44] and [23] for weight and size respectively. The circumferences were measured a the height of the RArmFront marker and the RightForeArm markers for upper arm and forearm, respectively. Thereby, muscles were relaxed. The weight is reported including the cloths worn during the experiments.

		Sex	Height (m)	Weight (kg)	UA Circ. (m)	FA Circ. (m)
♦	P_1	f	1.73	64.8	0.27	0.25
■	P_2	m	1.77	70	0.32	0.275
▲	P_3	m	1.80	83.9	0.33	0.295
●	P_4	m	1.85	70	0.27	0.26
[23], [44]	5th	f	1.489	49.4	0.218	0.199
	50th	-	1.685	70.1	0.284	0.261
	95th	m	1.901	96.4	0.351	0.327

The three dummy arm segments were sequentially attached to the SAAM to evaluate the diameter adaption. The motion capture system was used to determine the relative position of the attached dummies w.r.t. the base structure of the SAAM h_A. A caliper was used to measure D_{SAAM} for each attached dummy arm segment.

V. Case Study on Four Participants

To evaluate the performance of the attachment concepts in interaction with humans, we performed a case study series with four participants without upper limb impairment. The protocol of the case study was designed to evaluate the HRA systems with metrics that are independent of specific applications for exoskeletons (*e.g.*, neurotherapy, power-augmentation, assistance, and haptic rendering). Thereby, we strove for maximum transferability of the learnings to different application cases.

A. Participants and Initial Setup

The experiment protocol was approved by the ETH Zurich ethics commission (EK2021-N-185). All participants provided written, informed consent prior to the experiments. All methods were performed in accordance with the Declaration of Helsinki.

The system expert (*i.e.*, developer of the robot) thoroughly adjusted the robot segment lengths to fit each participant before the following experiments. Once the participant did not report any pulling on the joints when moving with the robot and sliding attachments were not observable, the *initial alignment* was achieved. The pose of robot and human were recorded using the motion capture system to be used as a reference for an optimal alignment with the corresponding attachment concept.

The four participants $P_i, \in \{1, 2, 3, 4\}$ were from a younger population (range 23 y to 31 y) of diverse heights mixed sex, and did not have an upper limb impairment (see Table II).

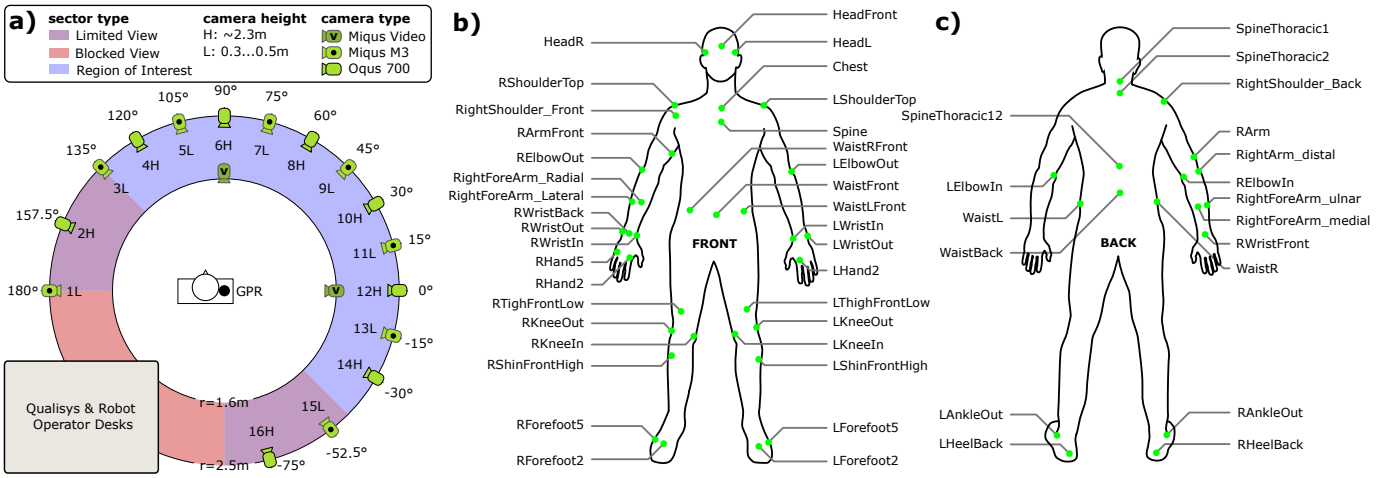

Fig. 6. Setup of motion capture measurement system; a) Arrangements of the marker tracking cameras (Oqus 700 and Miqus M3) and the synchronized video cameras Miqus Video (Qualisys AB, Sweden) w.r.t. the participant and exoskeleton; b) Marker locations on the front of the human; c) Marker locations on the back of the human.

B. Measurement Setup

Fifteen motion capture cameras and two synchronized video cameras (Qualisys AB, Sweden) were used to trace the markers attached to the participants and the robot (for details, see Fig. 6a and the supplemented material). To use the skeleton estimation function of Qualisys, the Sports Marker Set by Qualisys including markers on the lower limb and the head was required. However, due to the eminent occlusion by the robot, the marker set was extended (see Fig. 6b/c). The markers were glued to the skin of the participants by qualified personnel using Kinesiotape and screwed-in plastic bases without a spacer. The location of the markers was determined by palpation to locate anthropological landmarks, as described by the Qualisys instructions. Most of the markers on the robot were screwed to threads on the robot structure with dedicated location in CAD. Six markers on the robot were glued to the robot at measured locations (see supplementary material).

The sampling frequency of the system was set to 100 Hz for data acquisition, and the re-calibration was performed between sub-experiments to minimize position errors coming from the measurement system.

C. Data Processing and Evaluation

Qualisys Track Manager was used to post-process the acquired motion capture data. From the obtained data a skeleton model of the participants and rigid bodies of the exoskeleton was derived (see video[2]). Despite many motion capture cameras and view angles (see Fig. 6), there was missing data for some markers, which was necessary for further data analysis or to construct the model or the rigid bodies. The kinematic gap-filling feature was used, which estimates the missing marker positions based on the movements of a related skeleton segment or a rigid body. In addition, virtual markers were also generated using the 6-DOF bodies (*e.g.*, skeleton segments or rigid bodies) to acquire positions of certain human joints (e.g. GH joint).

A maximum torque control bandwidth of 5 Hz to 10 Hz was reported for humans [45]. Thus, a 2nd order Butterworth filter with a cut-off frequency of 7 Hz was used to filter the processed data from QTM before data analysis. The measured interaction wrenches were filtered by a second-order Butterworth filter with a cut-off frequency of 15 Hz for the upper arm and forearm sensors, and 20 Hz for the hand sensor.

Due to the limited cohort of four participants inter-participant statistical analysis was not applied.

[2]https://youtu.be/5WlXg7SJsCQ

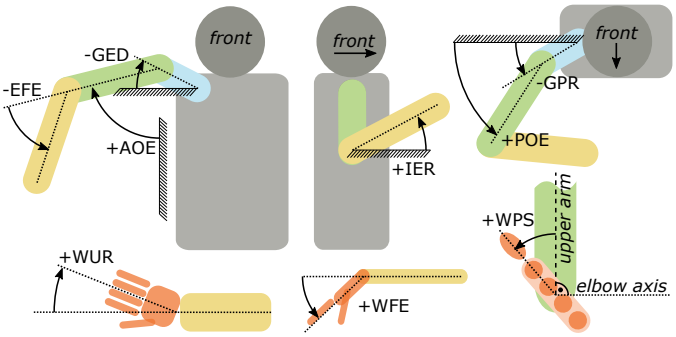

Fig. 7. Clinical joint coordinates with sign and neutral position definition: shoulder elevation(-)/depression(+) (GED), plane of elevation (POE), angle of elevation (AOE), internal(-)/external(+) shoulder rotation (IER), elbow flexion(-)/extension(+) (EFE), wrist pronation(-)/supination(+) (WPS), wrist flexion(+)/extension(-) (WFE), and wrist ulnar(+)/radial(-) bend (WUR).

D. Experiments of Case Study

1) Alignment Deflection Under Static Load: The relative deflection of the human joints w.r.t. the robot joints should be investigated during load transmission in a static position. The position control mode was used on the robot, and the position was set to the standard position (see Fig. 7 and Table III).

The participants were instructed to apply forces in the x- and y-directions of the UA-HRA and of the FA-HRA as much as they were able to or until the axial/radial forces and/or torques at each cuff (interaction points) reach 50 N and 15 N m, respectively. This procedure was repeated three times in each direction and for each HRA.

The human joint positions were evaluated during the loaded conditions by comparing the deflection of sternum (ST), glenohumeral joint (GH), elbow joint (EB), wrist joint (WR) and hand (HD) in the exoskeleton coordinate system (see

TABLE III
MOTIONS IN THE DOF LABELED WITH "MOV" WHILE THE OTHER DOF ARE IN THE REPORTED CONFIGURATION (TOP). POSITIONS FOR THE UNDESIRED CONTACT EXPERIMENT (BOTTOM): STANDARD POSE (STD), MIDDLE OF ROM (MID), HAND TO MOUTH (HTM), HAND REACHING HIGH (HRH).

	Arm Movement Configuration (in °)						
	POE	AOE	IER	EFE	WPS	WFE	WUR
hor. add./abd.	mov	90	35	90	0	0	0
add./abd.	90	mov	35	90	0	0	0
elev. frontal	90	mov	35	90	0	0	0
flex./ext.	100	mov	35	90	0	0	0
IER	90	50	mov	90	0	0	0
EFE	45	35-	0	mov	0	0	0
WPS	-	-	-	-	mov	0	0
WFE	-	-	-	-	0	mov	0
WUR	-	-	-	-	0	0	mov

	Arm Pose (in °)						
	POE	AOE	IER	EFE	WPS	WFE	WUR
Std	60	60	35	75	0	0	0
Mid	15	64	-19	72	0	0	0
Htm	79	55	42	112	24	-9	51
Hrh	78	125	47	53	3	-7	-57

Fig. 2b/c). To observe the deflection caused by loading the HRA separately from the misalignment due to the re-donning, the reference to compute the deflection was the equilibrium alignment condition before intentional loading was applied.

We assumed that after some movements the joint positions shift and stabilize at an equilibrium position. Therefore, we defined the default joint position vector, $\boldsymbol{p}_0$, as the point at which the interaction joint torques were smallest after the first movements. The interaction joint torques, $\boldsymbol{\tau}_{\text{int}}$, were calculated using the measured interaction wrenches, $\boldsymbol{\lambda}$, using

$$\boldsymbol{\tau}_{\text{int}} = \boldsymbol{J}_{\text{UA}}\boldsymbol{\lambda}_{\text{UA}} + \boldsymbol{J}_{\text{FA}}\boldsymbol{\lambda}_{\text{FA}} + \boldsymbol{J}_{\text{HD}}\boldsymbol{\lambda}_{\text{HD}} \tag{4}$$

where $\boldsymbol{J}$ is the spatial Jacobian and the subscripts indicate the interaction points.

For each of the reference points (ST, GH, EB, WR, and HD, see Fig. 2b/c), the peak deflection δ_{s}:

$$\delta_{\text{s}} = |\boldsymbol{p}_{t_F} - \boldsymbol{p}_0| \tag{5}$$

where $\boldsymbol{p}_{t_F}$ is the human joint position vector at the time t_F when maximum interaction forces were measured in the x- and y- axes of each cuff's coordinate system.

a) Alignment Deflection Under Dynamic Movements: The relative deflection of the human joints w.r.t. the robot joints should be investigated during dynamic movements. The robot was set to the damped free space control. The participants were instructed to perform nine different movements in a given order (see Table III top) by teach-and-repeat until they could perform the movement correctly. The participants slowly performed each movement, trying to achieve a ROM as large as possible, followed by two fast executions of the same movement.

The default joint position definition used in the 'static load' experiment could not be applied since the participants consistently interacted with the robot. Thus, the initial joint positions of the measured data from this experiment were used as the default joint position vector p_0.

For each of the reference points (ST, GH, EB, WR, and HD, see Fig. 2b/c), the peak deflection, δ_{d}, was determined for each performed movement:

$$\delta_{\text{d}} = \max\left(|\boldsymbol{p}_t - \boldsymbol{p}_0|\right) \tag{6}$$

where $\boldsymbol{p}_t$ is the human joint position vector at the time t.

For each participant, the range of motion in each joint was determined in the clinical coordinates (see Fig. 7). Thereof, the inter-participant median and standard deviation ROM was computed.

b) Establishing Undesired Contacts: This experiment should investigate the occurrence of undesired contacts between the robot and the human under load transfer in different static positions. For this experiment the robot was set to position control mode and the following positions were used (see Table III bottom):

- The standard position (used for initial alignment)
- The middle of the range of motion
- A posture of the arm when reaching to the mouth
- A posture simulating reaching to a high shelf

The robot was first moved to each joint position, before the participants were asked to establish contact at the shoulder and elbow sequentially. Two experiment instructors observed visually whether the participants were able to establish contact with the rigid structure of the robot. Contact at shoulder and/or elbow were documented and the interaction wrenches were measured.

The maximum net joint torques, τ_{max}, were obtained in order to evaluate how much interaction torques were required to make contacts:

$$\tau_{\text{max}} = \max\left(\boldsymbol{\tau}_{\text{int}}\right). \tag{7}$$

c) Attachment Repeatability: This experiment should investigate the consistency of the alignment when re-attaching the exoskeleton with external help and by self-attachment, thereby investigating the usability and consistency of the alignment. The robot's length settings remained from the initial setup, and the robot was set to the standard position.

For self-attachment, the participants were familiarized to donning and doffing the robot by tutoring of the expert prior to the experiment (three repetitions for $P_1 \ldots P_3$ and five for P_4). For the experiment, the participants donned and doffed two more times without tutoring. The positions of participant and robot were recorded by the motion capture system after each donning. Thereto, the participants were instructed to perform the attachment swiftly but accurately so that they could train with this attachment. The duration of donning for the self-attachment was measured by the instructor using a stopwatch beginning when the participants made contact with the chair (visually) until the participants stated attachment completion. The duration for doffing was measured from opening the first Velcro (auditory) to standing up from the seat (visually).

The participants were attached to the robot twice by a system expert and twice by a rookie to assess the re-attachment accuracy when an external person performs the attachment. The system expert instructed the rookie before the experiments and could train a couple of attachments before the experiment. However, the rookie did not perform more than 15 donning and

TABLE IV
MECHANICAL PROPERTIES OF THE SAAM. THE SAAM DIAMETER WAS MEASURED AT THE WIDEST POINT OF THE ALUMINUM WINGS. THE REPORTED STIFFNESS k_{MECH} INCLUDES THE COMPLIANCE OF THE 3 mm NEOPRENE PADDING AND THE DUMMY ARM SEGMENTS ITSELF. ΔM_{A} IS THE DEFLECTION OF THE MIDPOINT M_{A} OF THE DUMMY ARM SEGMENT FROM THE AVERAGE POSITION OF ALL THREE DUMMY ARM SEGMENTS.

dummy arm segment size		small	medium	large
D_{SAAM}	mm	101	117	134
Stiffness in x	N mm^{-1}	139	101	137
Stiffness in y	N mm^{-1}	49	37	37
$\Delta M_{\text{A,x}}$	mm	-0.4	0.2	0.2
$\Delta M_{\text{A,y}}$	mm	-0.2	0.6	-0.4

doffing cycles prior to the experiments. The motion capture system measured the participant's pose after each donning. The participants were instructed to sit straight and relax their arms.

The average pose of the participants during a 5 s record was compared to the average pose after the initial setup.

$$\bar{\boldsymbol{\delta}}_{\text{SA/RO/SE}} = \frac{1}{T}\sum_{t=0}^{T} \boldsymbol{p}_{\text{SA/RO/SE},t} - \boldsymbol{p}_{\text{init}} \tag{8}$$

where T is the measurement duration.

2) Overall Comfort: The overall comfort of the CAC and AAC was assessed by a modified Nordic questionnaire, where the participants could rate the discomfort on a visual analog scale for different body parts (see supplementary material). Further, the participants were asked to localize and comment any discomfort on a graphical visualization of the HRA. The questionnaires were filled at the end of of the corresponding experiment blocks with the AAC and the CAC.

3) Comfort During Biceps Contraction: The comfort of the two attachment systems during contraction of the biceps and the correlated cross-section change should be investigated in more detail. While the participants were attached to the robot, they were instructed to flex (90°) and extend (0°) their elbow three times. In the flexed position, the participants were instructed to contract their biceps brachii as much as possible. The experiment was documented with a camera to visualize the muscle deformation. After the experiment, the participants were asked to rate the perceived discomfort of each cuff system on a visual analog scale. The visual analog scales of these questionnaires were manually measured and documented to acquire quantitative values.

VI. RESULTS

A. Attachment Mechanism Properties

The measured stiffness of the UA-SAAM k_{mech} was higher than $101\,\text{N mm}^{-1}$ and $37\,\text{N mm}^{-1}$ in x- and y-direction of the SAAM, respectively for all three dummy arm segments (see Table IV). In comparison, the conventional UA cuff with a small cylindrical dummy arm segment and foam cushioning achieved a stiffness k_{mech} of $9\,\text{N mm}^{-1}$ and $19\,\text{N mm}^{-1}$ in x- and y-direction, respectively. The conventional UA attachment was too small for the large dummy arm segment, while the medium counterpart just fitted without cushioning.

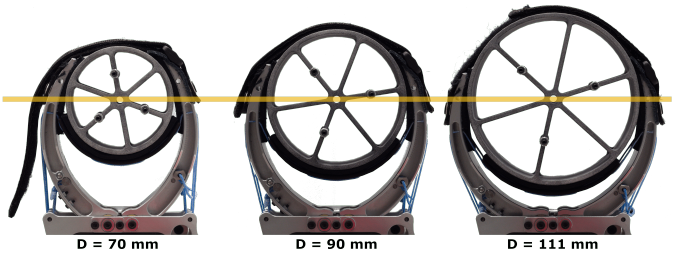

Fig. 8. Cylinders with a diameter varying from 70 mm to 111 mm attached to the mechanism were centered at the same distance h_A to the base structure with a deflection of less than 0.6 mm from the average position of all cylinder sizes.

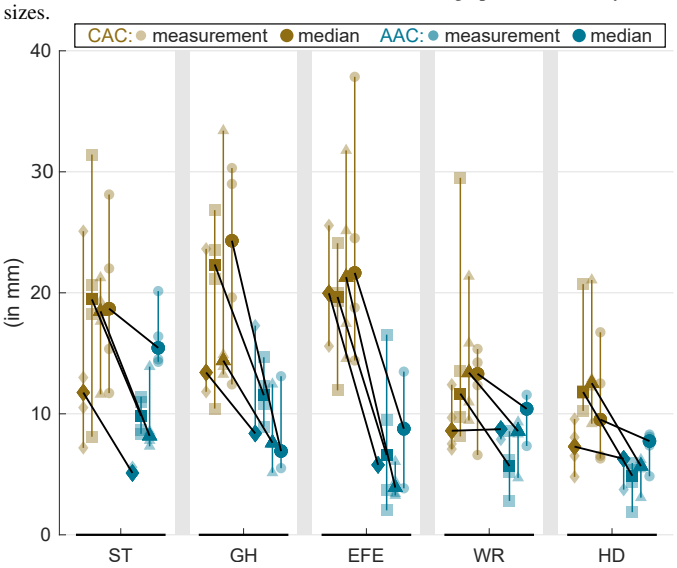

Fig. 9. Peak joint deflections under static loads of either 50 N or 15 N m on the interaction points, depending on which threshold was reached first.

The outer diameter of the SAAM adapted to each dummy arm segment such that the added diameter by the HRA compared to the diameter of the arm was 31 mm, 27 mm, and 23 mm, for small, medium, and large dummy arm segments, respectively (see Table IV and Fig. 8). The SAAM centered the different dummy arm segments with a difference of less than 0.7 mm and 1 mm from each other in x- and y-direction, respectively (see Fig. 8 and video[3]).

B. Alignment Deflection Under Static Load

During all static load cases, the peak deflection remained lower than 0.02 m when using the AAC, while values up to 0.04 m were observed for the CAC. The AAC showed a lower or equal intra-participant median deflection for all joints and participants. In average over all participants and joints, the deflection was reduced by 45 % when using the AAC and for the elbow joint the average inter-participant reduction was amounted to 70 %. For all reference points except ST, the intra-participant spread of the peak deflection was lower for the AAC (see Fig. 9) .

C. Alignment Deflection Under Dynamic Movements

For all reference locations, the observed peak deflections were lower for the AAC than for the CAC. Most intra-participant median peak deflections on ST, GH, and EB were

[3]https://youtu.be/-FB6mMNV_14

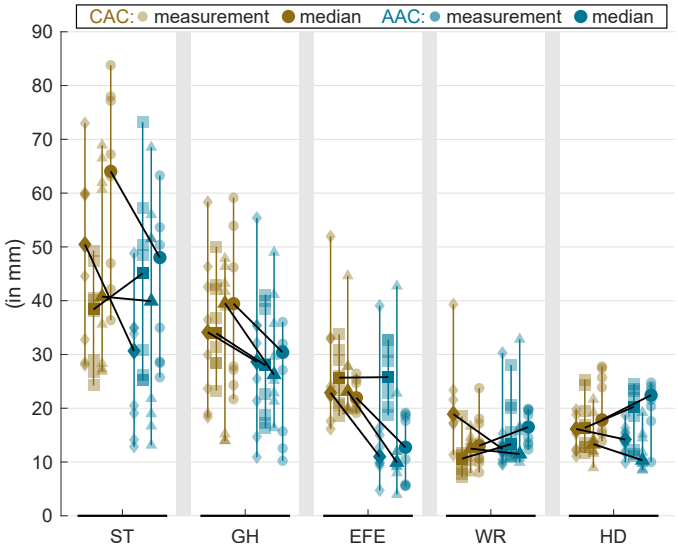

Fig. 10. Peak deflections occurring during "ROM movements" (Table III).

TABLE V
INTER-PARTICIPANT MEDIAN AND RANGE (*i.e.*, INTER-PARTICIPANT MAX DIFFERENCE) OF THE EXTREMAL JOINT POSITIONS IN CLINICAL COORDINATES THAT WERE REACHED DURING THE DYNAMIC MOVEMENTS. THE LARGER EXTREMA REACH PER JOINT IS HIGHLIGHTED GRAY.

	min pos. in °		max pos. in °	
	CAC	AAC	CAC	AAC
POE	-64.2 (15.6)	-66.1 (12.5)	152.8 (19.0)	149.8 (18.2)
AOE	11.9 (7.6)	15.9 (1.6)	142.7 (16.4)	151.4 (29.8)
IER	-19.1 (20.4)	-31.2 (29.6)	89.9 (10.8)	93.0 (26.8)
EFE	-129.4 (14.8)	-112 (24.1)	0.4 (11.2)	-2.3 (9.5)
WPS	-77.1 (65.5)	-68.3 (27.9)	81.6 (44.6)	88.9 (41.0)
WFE	-36.1 (24.6)	-48.7 (13.3)	69.0 (8.8)	68.9 (8.5)
WUR	-52.8 (19)	-45.1 (20.7)	36.1 (10.4)	36 (20.9)

lower for the AAC than for CAC (see Fig. 10).The inter-participant median range reached angles of elevation $4.3°$ closer to the body with the CAC than for the AAC. Similarly the range for elbow flexion was $16°$ larger for the CAC (see Table V).

D. Establishing Undesired Contact

For all trials with the AAC, the participants could only establish contact if they could establish the contact as well when using the CAC, except for participant P_4 and the *Mid* position. With the CAC, all participants could establish contact with the elbow at all arm postures, except P_2, who could not establish a contact in two of four arm poses. With the AAC, elbow contact could not be established in any condition. With the CAC, all participants except P_4 could establish contact with the shoulder in any arm pose, while for the AAC, only the *Mid* pose allowed the participants to establish contact reliably. For all trials, higher maximum interaction torques were established with the AAC. For 27 conditions (13 at the shoulder and 14 at the elbow), a contact was established with the CAC, 21 of these contacts were prevented by using the AAC (see Table VI).

E. Attachment Repeatability

On average, the intra-participant median deviation to the *initial alignment* at all reference points was smaller for the

TABLE VI
REPORTING OF UNDESIRED CONTACTS. A GRAY BLOCK AT THE TOP OR LOWER HALF OF A CELL INDICATES THAT A CONTACT WAS ESTABLISHED AT THE SHOULDER AND/OR ELBOW, RESPECTIVELY. IN THE CELL, THE MAXIMUM INTERACTION TORQUE τ_{MAX} (IN $\mathrm{N\,m}$) IS REPORTED WHICH WAS APPLIED DURING THE EXPERIMENT. AS SOON AS CONTACT WAS ESTABLISHED, THE PARTICIPANTS DID NOT INCREASE THE INTERACTION TORQUE FURTHER.

	CAC (in Nm)				AAC (in Nm)			
Pose	P_1	P_2	P_3	P_4	P_1	P_2	P_3	P_4
Std	14.9	20.6	10.4	N/A	18.1	33.6	11.2	38.1
Mid	10.6	14.0	10.4	N/A	22.8	17.7	11.7	40.2
Htm	8.2	14.0	8.5	N/A	9.7	14.7	13.0	47.4
Hrh	10.5	12.5	14.5	N/A	15.3	24.6	17.7	51.8

AAC independent of the person attaching. For ST and GH the inter-participant variance of the deviation was minor. Particularly the variation and accuracy of the ST and GH positioning by self-attachment was improved by the AAC (see Fig. 11). Peak deviations were lower for the AAC for all joints and people performing the attachment. All intra-participant median attachment deviations were lower or equal to $0.02\,\mathrm{m}$ for the sternum, glenohumeral joint, and elbow joint, except for the self-attachment of P_4 on the elbow. For wrist and hand, all alignment deviations were lower than $0.015\,\mathrm{m}$. For CAC, multiple intra-participant medians above $0.03\,\mathrm{m}$ were observed. Also, the peak offsets were higher for the CAC.

The outer diameter of the proximal UA-SAAM was smaller for participants P_1 and P_4 who had smaller UA-circumferences. For FA-SAAM the outer diameter settings for all attaching persons were in the strict order $P_1 < P_4 < P_2 < P_3$ (see Fig. 12). All donning trials took less than $65\,\mathrm{s}$ for CAC and less than $54\,\mathrm{s}$ for AAC. Doffing took less than $10\,\mathrm{s}$ for CAC and less than $11\,\mathrm{s}$ for the AAC. In average, the participants took $43\,\mathrm{s}$ to don and $8.3\,\mathrm{s}$ to doff (see Fig. 13 and video[4]).

F. Overall Comfort

The CAC was, in general, reported to be comfortable except for pinching of the textile belts at the proximal side of UA and FA cuffs. Participant P_2 and P_3 reported discomfort from compression at the upper arm. P_3 reported pinching at the proximal side of the CAC FA-HRA. P_2 reported pressure from the belt at the upper arm attachment.

For the AAC, all participants reported discomfort from the upper backrest after longer usage. All reported discomfort due to pinching at the proximal UA cuff. When flexing the elbow, two reported pinching between the distal UA-SAAM and the proximal FA-SAAM. P_2 reported pressure from the belt at the upper arm attachment and the proximal forearm attachment. Other discomfort on the forearm was not reported.

Only participant P_3 reported discomfort caused by the belt on the hand attachment for both the CAC and the AAC.

[4]https://youtu.be/RV003Zsxurk

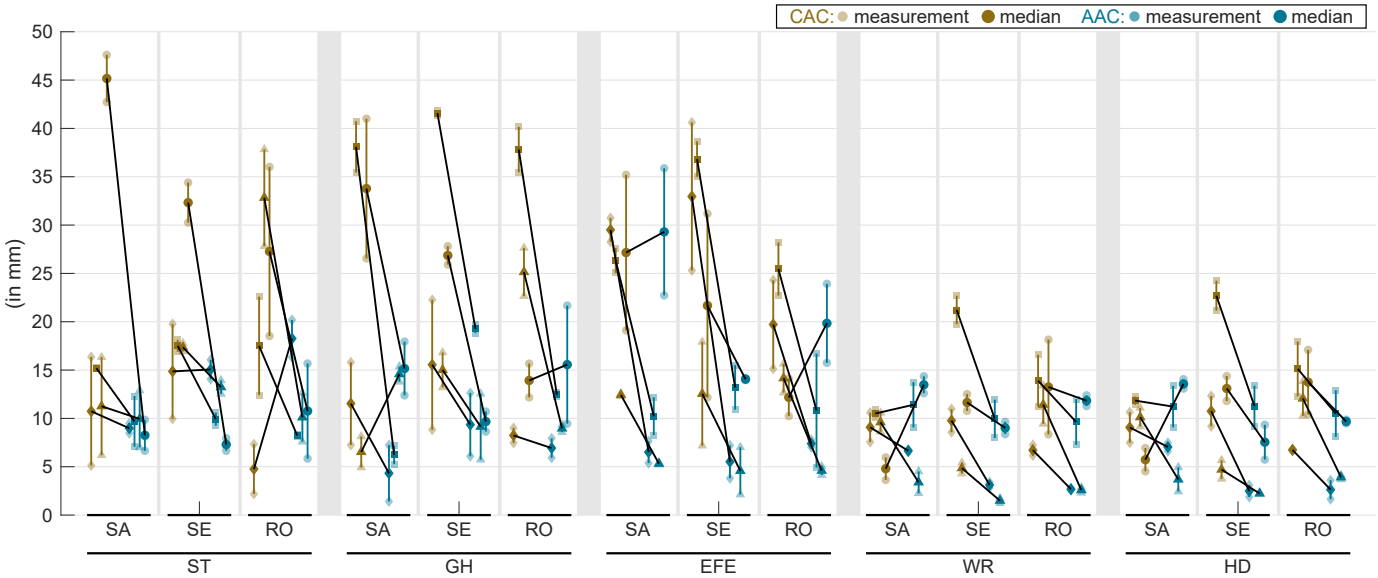

Fig. 11. Reattachment w.r.t. the position after the initial alignment performed by the self-attachment (SA), system expert (SE), and rookie (RO). Conventional attachment system (brown) and augmented attachment system (blue).

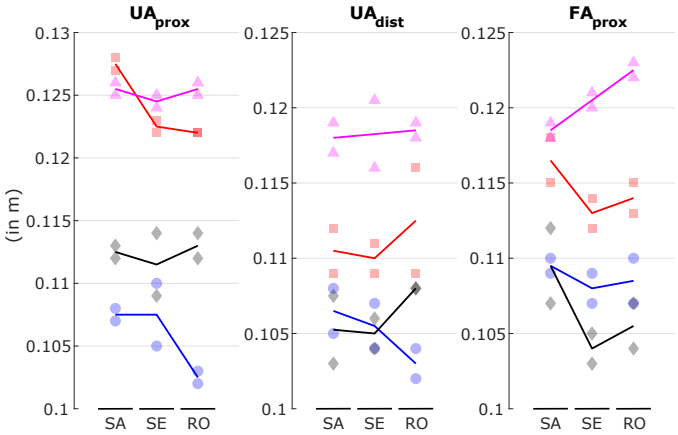

Fig. 12. Measured outer diameter of the cuff mechanism including the textile belts after attachment by self-attachment (SA), expert (SE), and rookie (RO).

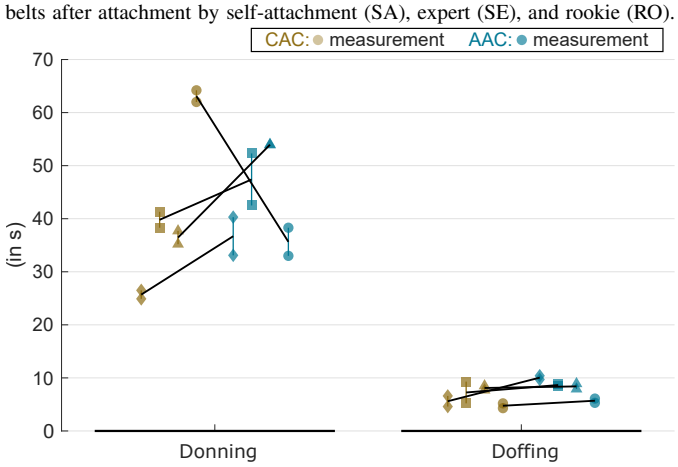

Fig. 13. Donning and doffing times for self-attachment. The black lines connect the intra-participant medians.

G. Comfort During Biceps Contraction

The biceps contraction was reported to be more comfortable when using the AAC. For the conventional cuff system higher amounts of discomfort were reported in the middle and distal part of the cuff (see Table VII).

TABLE VII
INTRA-PARTICIPANT MEDIAN AND MAXIMUM REPORTED DISCOMFORT (0: "NO DISCOMFORT"; 100: "EXTREME DISCOMFORT") AT THE PROXIMAL, MIDDLE AND DISTAL PART OF THE UPPER ARM ATTACHMENT.

	inter-part. median(max.)		
	proximal	middle	distal
CAC	10 (18)	7 (29)	13 (29)
AAC	9 (15)	0.6 (5)	7 (11)

VII. DISCUSSION

The experimental investigation of the relative movement between robot and human joints created quantitative insight into the magnitude of expected joint misalignment when re-attaching, during movements, and under load. Even when using the augmented attachment system, changes in the alignment of up to 15 mm on all joints frequently occur after re-attaching. Displacements in the same magnitude can occur when transmitting typical static interaction forces. Additionally, the experiment results highlight the strong influence of the attachment concept on the magnitude of misalignment and the occurrence of undesired contacts. This strong dependency reinforces the relevance of a sophisticated human-robot attachment design as the one proposed.

The augmented attachment system was designed to perform better regarding the design goals and requirements compared to conventional attachment systems. Therefore, we discuss the results relating to the requirement categories: A. Adaptability; B. Stiffness; C. Alignment Repeatability; D. Usability; E. Low Constraints on System.

A. Adaptability

Exoskeletons applied for neurotherapy are mostly shared devices. Hence, adaptability to different user sizes and shapes is essential, while the functionality and performance should be retained for all.

The SAAM adapted the outer diameter such that the attachment's footprint exceeded the small dummy arm segment

(5th percentile female) by only $15.5\,\mathrm{mm}$ on each side (see Table IV). A comparable fixed shell attachment mechanism with the outer dimensions of the SAAM, when fastened to a 95th percentile male arm, would exceed the 5th percentile female arm by $32\,\mathrm{mm}$ on each side. Thus, the SAAM adapted the footprint so that the protruding footprint for small arms was reduced by more than $50\,\%$ compared to a u-shaped mechanism that fits the same diameter range as the SAAM. A slimmer design of the SAAM should be possible. Hence, the relative reduction can be even higher.

This finding using the dummy arm segments was confirmed by the re-attachment experiment where the SAAM effectively lowered the attachment's footprint for the participants with thinner arms. Thereby, the ROM was increased for P_1 and P_4, as collisions between the attachment and the torso occured later than compared to a fixed footprint of the mechanisms.

The SAAM positioned the center of the three dummy arm segments at the same relative location with a maximum deviation of $1\,\mathrm{mm}$. Thus, compared to the theoretical offset of $22\,\mathrm{mm}$ without the automated alignment, the misalignment of the arm center was reduced by more than $95\,\%$ (see Table IV). Thereby, the robot and human joints can be aligned accurately independent of the user's arm diameter without additional cushioning or manual mechanism adaption (see video[5]).

B. Stiffness

A stiff connection between the human and robot arm segments benefits the retention of the joint alignment under load and helps prevent undesired contact points between the two. The stiffness properties of the attachment concepts were investigated regarding the mechanical components and the overall theoretical stiffness, including the human soft tissue.

1) Mechanical Stiffness: The SAAM's stiffness k_{mech} was consistently higher than $100\,\mathrm{N\,mm^{-1}}$ independent of which dummy arm segment was attached and was almost the same for the small and the large dummy arm segment. This consistency cannot be expected from a typical u-shaped attachment system where the thick cushioning layers for the smaller arms would strongly reduce the stiffness. The corresponding stiffness of the human soft tissue can be estimated to $k_{\text{SoftTissue,30}} = 3\,\mathrm{N\,mm^{-1}}$ based on the computations in section III-D. Due to the significantly higher stiffness of the SAAM w.r.t the corresponding soft tissue stiffness of humans, the serial stiffness of attachment will be dominated by the human tissue stiffness (see equation (1)).

2) Theoretical Overall Stiffness: On average, the two UA-SAAM were placed $0.121\,\mathrm{m}$ from each other for the four participants. Thus, according to equation (3) the AAC with the two $0.03\,\mathrm{m}$ wide SAAM achieves more than three times higher torsional stiffness in the x- and y-direction of the SAAM compared to the single $0.1\,\mathrm{m}$ wide UA attachment of the CAC. For this approximation, the assumption was made that the CAC stiffness depended only on the soft tissue stiffness which was rather optimistic for the CAC. These results provide information to estimate the effects of the gained stiffness on human-robot interaction control. We analyse the torsional stiffness in y-direction in more detail being the direction with the biggest difference in mechanical torsional stiffness between the AAC and CAC. Considering all stiffness contributions (see (1)) of the UA-HRA, the torsional stiffness of the AAC in y-direction was 5.3 times higher than for the CAC. Thus, the natural frequency of the coupled human-robot system is 2.3 times higher, approximating the human arm as a passive mass connected to the robot via this stiffness. Consequentially, interaction forces can be transmitted in a higher frequency band increasing the fidelity for haptic rendering and reducing the risk of exciting the natural frequencies of the coupled system (see video[6]). The increased bandwidth of interaction force transmission will lead to more direct feedback of the device in assistive and occupational applications (*i.e.*, improved control by the user) and for therapy and haptic-rendering applications it will allow rendering virtual realities including higher dynamics (*i.e.*, stiff walls). Furthermore, the increased stiffness reduces the phase delay for position control of the human arm in the frequency band that is relevant for therapy and mitigates the error in position estimation of the human arm. This estimation only considered a linear stiffness model, which approximated the system well for small interaction forces. However, for higher interaction forces, the soft tissue would be compressed and dislocated such that the stiffness increases progressively, resulting in a higher effective stiffness under high loads. These non-linear effects might have influenced the results of the practical experiments. However, the linear approximation around the operational point is exemplary for the considerations regarding system control.

3) Deflection Under Static Load and Resisted Dynamic Movement: The AAC prevented excessive misalignment under static load cases successfully with a maximum deflection of less than $0.02\,\mathrm{m}$ and an intra-participant median peak deflection of less than $0.01\,\mathrm{m}$ for all joints. These deflections are in the same range as the expected misalignment during the re-attachment (see Fig. 9 and Fig. 11). The CAC led to higher deflections on all joints where particularly the ST, GH, and EFE improved with the AAC.

During dynamic movements against resistance, the intra-participant median deflection and deflection spread were larger than for the static loads (see Fig. 10). We assume that the additional change in posture and less controlled generation of interaction forces between the robot and the human caused the increased movement. In some measurements, a shift of the estimated human joint position, estimated by Qualisys' skeleton tracking, w.r.t. the human shoulder was observed. This shift likely added distortion to the measurements. The upper arm joint locations GH and EB had less intra-participant median deflection during the dynamic movements when using the AAC. Thus, the AAC constrains the arm better during dynamic movements. The maximum deflections were lower for all joints with the AAC, indicating in general a more direct force transmission (*i.e.*, less phase delay) and less misalignment during usage with the AAC.

Even though the upper torso contact of the AAC interfaces with the back, the deflection of the sternum was reduced for

[5]https://youtu.be/-FB6mMNV_14

[6]https://youtu.be/RgazsS3NYpU

all participants in both load cases compared to not using the upper torso contact (CAC), except P_2 during the dynamic movements. This finding indicates that the upper torso promoted stabilization of the rotation around the vertical axis and constrains the lateral, dorsal, and ventral translation.

The consistently lower deflections of the glenohumeral and elbow joint locations with the AAC demonstrated the improved stiffness of the upper arm and forearm HRA, confirming the theoretical predictions. The additional support of the upper back likely contributed to the improved stiffness of the attachment. However, to guide the five SC and GH degrees of freedom of the human tightly, the 2-d force and 2-d torque support of the UA-HRA is essential.

The hand HRA with the open design towards the palmar side allows training of activities of daily living in real scenarios [15]. This realism should promote the transfer of skills acquired during therapy to daily living compared to pure virtual environment training [8]. The low deflections of the hand in the presence of static loads and movements against resistance indicate that the proposed hand attachment concept constrained sufficiently. Thus, real-world interactions and object manipulation are feasible while being supported by the device without sacrificing significant constraint quality. However, for training sessions involving high magnitude and alternating load transfer over the hand, we recommend using a conventional grip for a more natural loading of the hand.

Decreased relative movements between human and robot during operation will offer more control of the device to the human user in applications where the human dictates the movement. Thus, improved performance in safety-critical scenarios can be expected, *e.g.*, activity therapy exercises that involve movements proximal to the head of the user, and manipulating objects in a power-augmenting exoskeleton in a narrow environment.

4) Attempt to Establish Undesired Contacts: The increased stiffness of the AAC also reduced the risk of undesired contact points that spoil the interaction force measurement. The CAC constrained the elbow insufficiently, allowing the participants to easily establish contact with the robot in any arm posture. In contrast, the AAC prevented any elbow contacts reliably. This reliable elbow constraint is owed to the distal UA-SAAM and proximal FA-SAAM (see Table VI). The AAC prevented contact with the shoulder in half of the cases where the CAC failed, owing to the two contact points at the upper arm and the upper back constraint. The more muscular participants P_2 and P_3 could easily establish contact with the shoulder, as the gap between robot and skin was smaller. Furthermore, the thick layer of muscles between the attachment mechanism and the bone allowed to move more easily w.r.t. the attachment. Overall, the proposed attachment system reduced the occurrence of undesired contact points by $74\,\%$. Further, the maximum interaction torques reported in Table VI were consistently higher for the AAC than for CAC, indicating that the participants had to push more to establish contact, if possible. Hence, the AAC would prevent even more contact points when operating with lower interaction forces. Thus, measured interaction forces between robot and human are less likely to be disturbed by additional contacts when using the AAC. Thereby, any closed-loop control methods relying on precise interaction force measurement to track positions or torques will perform with much higher reliability, and less conservative parameters are required for safe operation.

To prevent all shoulder contacts, the exoskeleton parts would have to be placed at a higher distance to the user at the cost of higher inertia of the robot. Alternatively, the proximal UA-SAAM could be placed closer to the GH joint. However, the SAAM's footprint would have to be reduced further for a more proximal placement. We assume, that omitting the contact point either at the distal upper arm or at the proximal forearm would still result in a complete evasion of elbow contacts and could improve the range of motion in elbow flexion/extension (see Table V). To retain the constraint of the glenohumeral joint we recommend omitting the proximal forearm SAAM, if such a measure is striven for. Hence, there is a trade-off between ROM and stiffness.

C. Alignment Repeatability

Time-efficient and sufficiently accurate re-attachment of the exoskeleton to the user is essential for the clinical adoption of the device. The improved alignment accuracy for the ST, GH, and EFE with the AAC indicates that the upper torso constraint and the two SAAM per arm segment helped all people performing the attachment to align the participant's arm more consistently (see Fig. 11). The rookie profited the most from the AAC for the torso alignment. For the self-attachment with the AAC, the intra-participant median deviations were lower than $0.015\,\mathrm{m}$ for all joints, except for one outlier of P_4 at the elbow which could have been caused by a shifted marker. These values were often higher than $0.035\,\mathrm{m}$ when using the CAC. Hence, the consistency of self-alignment could be doubled by the AAC, making it more eligible as the difference to the assisted attachments was diminished.

For WR and HD the displacement seemed better with AAC for the expert and the rookie, while self-attachment was indifferent. The tactile feedback from distal forearm and hand attachment that the participants could leverage when fastening the same can explain the discrepancy between self and external attachment. Without this tactile feedback, the rookie and system expert seemed to benefit from the support of the proximal forearm attachment and the two SAAM at the upper arm when positioning the hand and wrist.

The low intra-attachment-person change in D_{SAAM} can be explained by the natural force feedback of the tightening process, which helped the attaching person to perform consistently. For the participants with the smaller arm circumference, the D_{SAAM} was smaller for all people performing the attachment, indicating that the diameter adaption works reliably independent of the attaching person (see Fig. 12).

Self-attachment was feasible for all participants after little training. Self-attachment, attachment by an expert, and attachment by instructed rookie led to a comparable accuracy of the alignment w.r.t. the initial alignment when using the AAC. Thus, self-alignment can be expected to lead to a similar quality of alignment as the attachment by external people. For therapy devices, the improved repeatability of the alignment

will increase the quality of longitudinal therapy assessments that rely on consistent conditions in the human-robot attachment. Further, learning to incorporate the characteristics of human-robot interaction into motor control skills will be easier for users of assistive and occupational devices.

The participants required in average less than $52\,\mathrm{s}$ to don and doff the device with the AAC, which is by far quicker than our requirement. The CAC was slightly faster to don and doff due to the fewer straps that had to be closed (see Fig. 13). The arm attached to the robot does not contribute actively to the self-attachment procedure. Thus, to enable self-attachment, the only additional criterion for the patient is that they can place and hold their affected arm in the device. The robot could assist the user by individualized donning postures.

D. Usability

The attachment system was completely accessible without the need to maneuver the hand through confined spaces. Therefore, we expect the HRA to be well suited for severely affected patients even though they might rely on external help to don the device. The successful self-attachments of all participants demonstrated reliable one-handed operation. In addition to self-alignment, the one-handed operation allows people who assist a patient in donning the device to use one hand to position the patient's arm. The hand attachment was designed so that objects could be grasped, while providing a sufficient constraint (*i.e.*, low deflections). The upper backrest improved the stability of the torso position without strapping the torso to the structure. Thus, torso stability can be trained while using the robot. Neither tools nor additional items were used to adapt the proposed attachment system to the users. Easy self-attachment is particularly beneficial in exoskeletons for assistance in daily life and occupational tasks.

E. Low Constraints on System

For the HRA concept to be adopted in clinical practice, it may only marginally restrict the system's performance regarding comfort, range of motion, and inertia.

1) Comfort: The AAC allowed cross-section changes of the biceps during elbow flexion, which was observed visually (see video[7]) and reflected in the subjective comfort rating of the participants. During the biceps contraction experiment the distal UA-SAAM still caused slight discomfort due to pressure on the tendons. However, the overall comfort rating during biceps flexion was better for the ACC than for the CAC, particularly for the participants with wider arm circumference (see Table VII). The increased comfort of the AAC can be explained by the improved admittance to cross-section changes of the muscles and the lower torsional stiffness of the individual SAAM compared to the CAC. Placing the distal UA-SAAM closer to the elbow would further improve the comfort during biceps flexion. However, in this case the proximal FA-SAAM should be placed more distal to prevent a reduction of the elbow ROM.

[7]https://youtu.be/tPzSTW_Nc6U

For the overall comfort of the two attachment concepts, the participants reported less discomfort for the CAC than for the AAC. However, simple design improvements on the AAC could mitigate the comfort problems:

- The AAC was not designed for use without a clothing layer. To attach the markers the participants wore only a muscle shirt leaving the arm unprotected. Working with the prototype has shown, that wearing a long sleeved sports shirt or pullover would mitigate the pinching issue.
- The printed bars of the upper backrest had a rather rough surface with barely rounded edges. Designing them with larger radii and a smooth, slightly compliant surface covering, *e.g.*, silicon, is expected to solve the issue.
- During the experiments, the proximal FA-SAAM was placed close to the elbow. Together with the distal UA-SAAM, pinching occurred for some participants. We recommend placing the proximal FA-SAAM further from the elbow to prevent this issue or completely omitting this attachment point. The proximal FA-SAAM helped to distribute the transmitted forces more evenly and thereby reduced the pressure on the skin and increased the stiffness of the connection. However, the overall performance of the exoskeleton might benefit more from preventing the pinching issue than the added stiffness.
- The improved torsional stiffness at the upper arm made a mismatch between the implemented and the physiological SC-coupling of the user more perceivable. Customizing the nominal coupling function or a lower impedance might improve the comfort.

2) Range of Motion: Placing the two contact points close to the proximal and distal end of the forearm and upper arm has improved the stiffness remarkably. However, the concern was that the attachment mechanisms close to the armpit and the elbow could restrict the ROM. The results show indeed that with the AAC the ROM for low angles of elevation was reduced by 4° compared to CAC (see Table V). Nevertheless, the inter-participant maximum difference is around a factor of five lower for the AAC, which indicates that the ROM is more consistent for all users. We assume that the adaptable footprint of the SAAM allowed the smaller participants to reach the same ROM as the taller participants. The reached elbow flexion was lower for the AAC, which is probably the most noticeable drawback. In other directions, the AAC even allowed for a more extensive range.

3) Inertia: The weight of the HRA was $570\,\mathrm{g}$, $227\,\mathrm{g}$, and $247\,\mathrm{g}$ for upper arm, forearm and hand attachment, respectively, which is lightweight compared to the functionality. However, conventional HRA systems tend to be lighter.

VIII. Conclusion

A. Discussion Summary

Adaptablility: The attachment system was adaptable for the 5th percentile female to the 95th percentile male concerning arm segment length and diameter. As the recruited participants were rather tall, the functionality could not be evaluated for people close to the 5th percentile female body height within this study.

Stiffness: The proposed augmented attachment concept reduced the relative joint deflections under load and mitigated the occurrence of undesired contacts remarkably compared to the conventional attachment system (see Fig. 9 and 10). Thus, parasitic loads on the human joints will be reduced, and precision of human joint angle measurements will be increased. In addition, the system facilitates improving the accuracy and transmission bandwidth of closed-loop interaction force control.

Alignment Repeatability: The re-attachment with the augmented attachment concept achieved similar discrepancies compared to the initial alignment independent of who executed the attachment procedure and remarkably better performance than the conventional attachment concept. Thus, time-efficient self-attachment is possible with a comparable alignment result to an expert attaching.

Usability: The proposed mechanism can be operated with one hand. Thus, self-attachment should be possible given sufficient functionality of the contra-lateral limb. Further, no tools or exchangeable parts are required to adapt the mechanism to different patients, making the use in clinical settings highly efficient. Easy self-attachment with automated adaption to different limb diameters enables fast deployment of shared devices in occupational, therapy, and haptic-rendering applications.

Low Constraints on System: The SAAM kept the footprint of the attachment mechanism low. Thus, the attachment points can be placed closer to the GH and EB joint without significantly reducing the ROM. The comfort of the proposed attachment system was sufficient for acceptable comfort ratings after wearing and using the device for at least $1\,\mathrm{h}$. Thus, we deem the system applicable. However, the suggested improvements on the design of the attachment system should be implemented to match up with the comfort of conventional systems.

B. Limitations

The presented study considered two conditions (AAC and CAC). This limited the conclusions that can be derived regarding the individual influence of the suggested design, *e.g.*, SAAM vs. multiple contact points per limb segment. The mathematical analysis of the stiffness contributions in III-D indicated a shared contribution of the two design elements from the example. To quantify the contributions of individual elements of the HRA, we suggest a study comparing more granular modifications to the design choice. Testing on a larger cohort with optimized protocol might be interesting to apply inter-participant statistics. However, due to the large number of required markers on the human and robot arms, the post-processing of the motion capture involves labor-intensive manual labeling. For such a study, we recommend limiting the static postures and movements to a subset that enables reliable automated marker labeling. Evaluating the AAC's performance for the target patient population- and investigating shear forces at the HRA should be addressed in future research, *e.g.*, self-attachment.

C. Contribution

We introduced an augmented human-robot attachment system for upper limb exoskeletons. The system consisted of a tactile positioning aid for the upper torso, two contact points on the forearm and upper arm, realized by a self-adapting attachment mechanism, and a hand attachment allowing to grasp objects. The proposed attachment system unified stiff constraints and consistent joint alignment with a slim and easy-to-use design, as shown by the case study with four participants. The results indicate, that the proposed system performed better than a conventional attachment system regarding alignment accuracy, repeatability, and stiffness of the human-robot connection. The substantially increased stiffness of the human-robot attachment lowers the phase delay between the dynamics of the human and robot arms and enables accurate interaction force measurement by preventing undesired contacts of the arms. Thus, the proposed system will benefit high-performance interaction force control. The improved consistency of the stiffness between different users compared to conventional systems will allow more performance-oriented tuning of said control algorithms. The improved accuracy, repeatability, and retention of the alignment allow for a more consistent and accurate estimation of the human arm's position leading to more reliable monitoring and assessments. Furthermore, the attachment concept enables fast donning and doffing of the device, even by self-attachment without requiring any tools or parts customized for individual users. To the authors' knowledge, these features were so far not unified in one attachment concept. The proposed concept, with minor design modification, can easily be transferred to other upper and lower limb exoskeletons including applications for power augmentation (*e.g.*, automotive industry, defense), daily life assistance (*e.g.*, mobility), entertainment (*e.g.*, haptic rendering), telemanipulation (*e.g.*, construction), and rehabilitation (*e.g.*, neurotherapy). Thus, our contribution addresses a key feature of exoskeleton design applicable to a broad field of applications.

Acknowledgment

The authors thank Patrick Huwiler, Florian Teuscher, Patrick Bösch, Anna-Maria Georgarakis, Marco Bader, and Matthew Hanlon for their valuable support of our research.

References

[1] M. P. Lindsay, B. Norrving, R. L. Sacco, M. Brainin, W. Hacke, S. Martins, J. Pandian, and V. Feigin, "World stroke organization (wso): global stroke fact sheet 2019," 2019.

[2] V. L. Feigin, E. Nichols, T. Alam, M. S. Bannick, E. Beghi, N. Blake, W. J. Culpepper, E. R. Dorsey, A. Elbaz, R. G. Ellenbogen *et al.*, "Global, regional, and national burden of neurological disorders, 1990–2016: a systematic analysis for the global burden of disease study 2016," *The Lancet Neurology*, vol. 18, no. 5, pp. 459–480, 2019.

[3] S. A. Combs, S. P. Kelly, R. Barton, M. Ivaska, and K. Nowak, "Effects of an intensive, task-specific rehabilitation program for individuals with chronic stroke: A case series," *Disability and Rehabilitation*, vol. 32, no. 8, pp. 669–678, jan 2010.

[4] K. Wing, J. V. Lynskey, and P. R. Bosch, "Whole-Body Intensive Rehabilitation Is Feasible and Effective in Chronic Stroke Survivors: A Retrospective Data Analysis," *Topics in Stroke Rehabilitation*, vol. 15, no. 3, pp. 247–255, 2008.

[5] G. Kwakkel, B. J. Kollen, J. V. Van der Grond, and A. J. H. Prevo, "Probability of regaining dexterity in the flaccid upper limb: Impact of severity of paresis and time since onset in acute stroke," *Stroke*, vol. 34, no. 9, pp. 2181–2186, 2003.

[6] L. H. Thomas, B. French, J. Coupe, N. McMahon, L. Connell, J. Harrison, C. J. Sutton, S. Tishkovskaya, and C. L. Watkins, "Repetitive Task Training for Improving Functional Ability after Stroke: A Major Update of a Cochrane Review," *Stroke*, vol. 48, no. 4, pp. e102–e103, 2017.

[7] J. Bo Nielsen, M. Willerslev-Olsen, L. Christiansen, J. Lundbye-Jensen, and J. Lorentzen, "Science-based neurorehabilitation: Recommendations for neurorehabilitation from basic science," *Journal of Motor Behavior*, vol. 47, no. 1, pp. 7–17, 2015.

[8] V. Klamroth-Marganska, J. Blanco, K. Campen, A. Curt, V. Dietz, T. Ettlin, M. Felder, B. Fellinghauer, M. Guidali, A. Kollmar, A. Luft, T. Nef, C. Schuster-Amft, W. Stahel, and R. Riener, "Three-dimensional, task-specific robot therapy of the arm after stroke: A multicentre, parallel-group randomised trial," *The Lancet Neurology*, 2014.

[9] Y. Zimmermann, A. Forino, R. Riener, and M. Hutter, "ANYexo: A Versatile and Dynamic Upper-Limb Rehabilitation Robot," *IEEE Robotics and Automation Letters*, oct 2019.

[10] B. Kim and A. D. Deshpande, "An upper-body rehabilitation exoskeleton Harmony with an anatomical shoulder mechanism: Design, modeling, control, and performance evaluation," *The International Journal of Robotics Research*, 2017.

[11] T. Nef, M. Guidali, and R. Riener, "ARMin III – arm therapy exoskeleton with an ergonomic shoulder actuation," *Applied Bionics and Biomechanics*, vol. 6, no. 2, pp. 127–142, 2009.

[12] V. Bartenbach, "Constraints caused by lower extremity exoskeletons," Ph.D. dissertation, ETH Zurich, 2017.

[13] N. Jarrassé and G. Morel, "Connecting a human limb to an exoskeleton," *IEEE Transactions on Robotics*, vol. 28, no. 3, pp. 697–709, 2011.

[14] A. Otten, C. Voort, A. Stienen, R. Aarts, E. Van Asseldonk, and H. Van Der Kooij, "LIMPACT:A Hydraulically Powered Self-Aligning Upper Limb Exoskeleton," *IEEE/ASME Transactions on Mechatronics*, 2015.

[15] Y. Zimmermann, M. Sommerhalder, P. Wolf, R. Riener, and M. Hutter, "Anyexo 2.0: A fully actuated upper-limb exoskeleton for manipulation and joint-oriented training in all stages of rehabilitation," *IEEE Transactions on Robotics*, pp. 1–20, 2023.

[16] J. C. Perry, J. Rosen, and S. Burns, "Upper-limb powered exoskeleton design," *IEEE/ASME Transactions on Mechatronics*, 2007.

[17] Y. Mao and S. K. Agrawal, "Design of a cable-driven arm exoskeleton (CAREX) for neural rehabilitation," *IEEE Transactions on Robotics*, 2012.

[18] A. Gupta and M. K. O. Malley, "Robotic Exoskeletons for Upper Extremity Rehabilitation," *Rehabilitation Robotics*, vol. 1, no. August, pp. 648–674, 2006.

[19] M. B. Näf, K. Junius, M. Rossini, C. Rodriguez-Guerrero, B. Vanderborght, and D. Lefeber, "Misalignment compensation for full human-exoskeleton kinematic compatibility: state of the art and evaluation," *Applied Mechanics Reviews*, vol. 70, no. 5, 2018.

[20] M. Cempini, S. M. M. De Rossi, T. Lenzi, N. Vitiello, and M. C. Carrozza, "Self-alignment mechanisms for assistive wearable robots: A kinetostatic compatibility method," *IEEE Transactions on Robotics*, vol. 29, no. 1, pp. 236–250, 2012.

[21] Y. Zimmermann, "A versatile upper-limb exoskeleton for neurorehabilitation," Ph.D. dissertation, ETH Zurich, 2022.

[22] E. Churchill and J. T. McConville, "Sampling and data gathering strategies for future usaf anthropometry," 1976.

[23] "National aerospace and space administration: Anthropometry and biomechanics," https://msis.jsc.nasa.gov/sections/Section03.htm, accessed: 2022-04-14.

[24] Y. Zimmermann, E. B. Küçüktabak, F. Farshidian, R. Riener, and M. Hutter, "Towards dynamic transparency: Robust interaction force tracking using multi-sensory control on an arm exoskeleton," in *2020 IEEE/RSJ International Conference on Intelligent Robots and Systems (IROS)*. IEEE, 2020, pp. 7417–7424.

[25] E. Pirondini, M. Coscia, S. Marcheschi, G. Roas, F. Salsedo, A. Frisoli, M. Bergamasco, and S. Micera, "Evaluation of the effects of the arm light exoskeleton on movement execution and muscle activities: a pilot study on healthy subjects," *Journal of neuroengineering and rehabilitation*, vol. 13, no. 1, pp. 1–21, 2016.

[26] D. J. Hyun, H. Park, T. Ha, S. Park, and K. Jung, "Biomechanical design of an agile, electricity-powered lower-limb exoskeleton for weight-bearing assistance," *Robotics and Autonomous Systems*, vol. 95, pp. 181–195, 2017.

[27] G. Yang, H. L. Ho, W. Chen, W. Lin, S. H. Yeo, and M. S. Kurbanhusen, "A haptic device wearable on a human arm," in *IEEE Conference on Robotics, Automation and Mechatronics, 2004.*, vol. 1. IEEE, 2004, pp. 243–247.

[28] A. Schiele, "Ergonomics of exoskeletons: Objective performance metrics," *Proceedings - 3rd Joint EuroHaptics Conference and Symposium on Haptic Interfaces for Virtual Environment and Teleoperator Systems, World Haptics 2009*, pp. 103–108, 2009.

[29] R. Soltani-Zarrin, A. Zeiaee, R. Langari, and R. Tafreshi, "Robotic upper limb rehabilitation device," Jul. 4 2019, uS Patent App. 16/298,777.

[30] A. Schiele and G. Visentin, "Exoskeleton for the human arm, in particular for space applications," Aug. 12 2008, uS Patent 7,410,338.

[31] A. Schiele and F. C. Van der Helm, "Influence of attachment pressure and kinematic configuration on phri with wearable robots," *Applied Bionics and Biomechanics*, vol. 6, no. 2, pp. 157–173, 2009.

[32] J. Restrepo-Zapata, C. Gallego-Duque, D. Marquez-Viloria, and J. Botero-Valencia, "Two-degree adjustable exoskeleton for assistance of the human arm using a mechanical system of fast assembly and upgradability." *International Journal on Smart Sensing & Intelligent Systems*, vol. 10, no. 3, 2017.

[33] W. Chen, Z. Li, X. Cui, J. Zhang, and S. Bai, "Mechanical design and kinematic modeling of a cable-driven arm exoskeleton incorporating inaccurate human limb anthropomorphic parameters," *Sensors*, vol. 19, no. 20, p. 4461, 2019.

[34] X. Cui, W. Chen, X. Jin, and S. K. Agrawal, "Design of a 7-dof cable-driven arm exoskeleton (carex-7) and a controller for dexterous motion training or assistance," *IEEE/ASME Transactions on Mechatronics*, vol. 22, no. 1, pp. 161–172, 2016.

[35] N. Vitiello, T. Lenzi, S. Roccella, S. M. M. De Rossi, E. Cattin, F. Giovacchini, F. Vecchi, and M. C. Carrozza, "Neuroexos: A powered elbow exoskeleton for physical rehabilitation," *IEEE transactions on robotics*, vol. 29, no. 1, pp. 220–235, 2012.

[36] A. Zoss, H. Kazerooni, and A. Chu, "On the mechanical design of the berkeley lower extremity exoskeleton (bleex)," in *2005 IEEE/RSJ international conference on intelligent robots and systems*. IEEE, 2005, pp. 3465–3472.

[37] J. Rosen, J. C. Perry, N. Manning, S. Burns, and B. Hannaford, "The human arm kinematics and dynamics during daily activities - Toward a 7 DOF upper limb powered exoskeleton," *2005 International Conference on Advanced Robotics, ICAR '05, Proceedings*, vol. 2005, no. July, pp. 532–539, 2005.

[38] U. Keller, H. J. Van Hedel, V. Klamroth-Marganska, and R. Riener, "ChARMin: The First Actuated Exoskeleton Robot for Pediatric Arm Rehabilitation," *IEEE/ASME Transactions on Mechatronics*, vol. 21, no. 5, pp. 2201–2213, 2016.

[39] M. Mihelj, T. Nef, and R. Riener, "ARMin II - 7 DoF rehabilitation robot: Mechanics and kinematics," *Proceedings - IEEE International Conference on Robotics and Automation*, no. April, pp. 4120–4125, 2007.

[40] S. Jijun, Z. Haitian, and G. Tongtong, "The study of mechanical properties on soft tissue of human forearm in vivo," *3rd International Conference on Bioinformatics and Biomedical Engineering, iCBBE 2009*, pp. 8–11, 2009.

[41] J. Iivarinen, *Diagnostics of human forearm soft tissues using indentation and suction measurements: experimental and modeling analysis*. Itä-Suomen yliopisto, 2014.

[42] H. Haapasalo, H. Sievanen, P. Kannus, A. Heinonen, P. Oja, and I. Vuori, "Dimensions and estimated mechanical characteristics of the humerus after long-term tennis loading," *Journal of Bone and Mineral Research*, vol. 11, no. 6, pp. 864–872, 1996.

[43] A. H. Murdoch, K. Mathias, and F. Smith, "Measurement of the bony anatomy of the humerus using magnetic resonance imaging," *Proceedings of the Institution of Mechanical Engineers, Part H: Journal of Engineering in Medicine*, vol. 216, no. 1, pp. 31–35, 2002.

[44] R. L. Huston, *Principles of biomechanics*. CRC press, 2008.

[45] T. L. Brooks, "Telerobotic response requirements," *Systems, Man and Cybernetics, 1990. Conference Proceedings., IEEE International Conference on*, 1990.